

# Spreading characteristics of compressible jets from nozzles of various geometries

By K. B. M. Q. ZAMAN

NASA Lewis Research Center, Cleveland, OH 44135, USA

(Received 25 November 1997 and in revised form 22 October 1998)

The spreading characteristics of jets from several asymmetric nozzles, and a set of rectangular orifices are compared, covering a jet Mach number range of 0.3–2.0. The effect of ‘tabs’ for a rectangular and a round nozzle is also included in the comparison. Compared to a round jet, the jets from the asymmetric nozzles spread only slightly more at subsonic conditions whereas at supersonic conditions, when ‘screech’ occurs, they spread much more. The dynamics of the azimuthal vortical structures of the jet, organized and intensified under the screeching condition, are thought to be responsible for the observed effect at supersonic conditions. Curiously, the jet from a ‘lobed’ nozzle spreads much less at supersonic condition compared to all other cases; this is due to the absence of screech with this nozzle. Screech stages inducing flapping, rather than varicose or helical, flow oscillation cause a more pronounced jet spreading. At subsonic conditions, only a slight increase in jet spreading with the asymmetric nozzles contrasts previous observations by others. The present results show that the spreading of most asymmetric jets is not much different from that of a round jet. This inference is further supported by data from the rectangular orifices. In fact, jets from the orifices with small aspect ratio ( $AR$ ) exhibit virtually no increase in the spreading. A noticeable increase commences only when  $AR$  is larger than about 10. Thus, ‘shear layer perimeter stretching’, achieved with a larger  $AR$  for a given cross-sectional area of the orifice, by itself, proves to be a relatively inefficient mechanism for increasing jet spreading. In contrast, the presence of streamwise vortices or ‘natural excitation’ can cause a significant increase – effects that might explain the observations in the previous investigations. Thus far, the biggest increase in jet spreading is observed with the tabs. This is true in the subsonic regime, as well as in the supersonic regime, in spite of the fact that screech is eliminated by the tabs. The characteristic spreading of the tabbed jets is explained by the induced motion of the tab-generated streamwise vortex pairs. The tabs, however, incur thrust loss; the flow blockage and loss in thrust coefficient, *vis-à-vis* the spreading increase, are evaluated for various configurations.

---

## 1. Introduction

It has been observed that jets from asymmetric nozzles spread and mix faster than their axisymmetric counterparts. For example, Ho & Gutmak (1987) and Hussain & Husain (1989) had shown that the overall spreading of small aspect ratio elliptic jets was clearly more than that of an axisymmetric jet. There were many studies on jets from rectangular nozzles (Trentacoste & Sforza 1967; Krothapalli *et al.* 1981; Tsuchiya, Horikoshi & Sato 1986; Grinstein 1995) some of which also indicated more vigorous entrainment characteristics. While most of these observations were

made with low Mach number subsonic jets, a similar inference was also made for supersonic elliptic jets (Schadow *et al.* 1987).

A more complex asymmetric geometry is that of a 'lobed' nozzle designed to increase mixing (see e.g. McCormick & Bennett 1993; Belovich, Samimy & Reeder 1996). Here, the primary concept is to stretch the perimeter of the shear layer exposed to the ambient so that more entrainment takes place. However, apart from this 'shear layer perimeter stretching', often streamwise vorticity is introduced in the jet when using lobed or other asymmetric nozzles. This can occur owing to secondary flow upstream within the nozzle (see e.g. Bradshaw 1987), or by deliberate vectoring of the flow from alternate lobes. Another technique for introducing streamwise vortices, receiving renewed attention in recent years involves the use of vortex generators in the form of 'tabs' (Ahuja & Brown 1989; Zaman, Reeder & Samimy 1994; Zhang & Schneider 1995; Surks, Rogers & Parekh 1994; Bohl & Foss 1996; Reeder & Samimy 1996; Reeder & Zaman 1996; Foss & Zaman 1999). A tab is a small protrusion placed at the jet nozzle exit that produces a pair of counter-rotating vortices. These 'steady-state' streamwise vortex pairs, manifested even on the time-averaged flow field, can have a profound impact on the spreading of the jet and explain many features of the overall jet evolution (Zaman 1996*b*). That streamwise vortex pairs, occurring in the instantaneous flow field of a jet, play a significant role in the entrainment process was shown by Liepmann & Gharib (1992). The effect of forced unsteadiness affecting jet evolution has also been addressed by Lasheras & Prestridge (1997) for a lobed nozzle, and by Zaman & Raman (1997) for a tabbed nozzle.

Based on the data available from the literature, however, a direct comparison of the spreading characteristics of jets from the various nozzle configurations has been difficult. This can be appreciated from the data, tabulated by Gutmak, Schadow & Yu (1995), based on past work on mixing enhancement in free shear flows. Part of the difficulty stems from the fact that jet spreading can be defined in a number of ways, and different studies have used different parameters for that purpose. Many parameters, such as streamwise variation of the jet half-velocity-width or the centreline velocity, would only provide a partial description and, sometimes, could even be misleading. Another difficulty arises owing to differences in operating conditions in the previous studies, especially in Mach number. It is well known that mixing layer spreading decreases with increasing compressibility at higher Mach numbers (Papamoschou & Roshko 1988). Therefore, a comparison of the jet spreading with different nozzles might be meaningful only when carried out at comparable Mach numbers and preferably based on the measurement of the entire flow field. The purpose of the present investigation is to carry out such a comparative evaluation.

Only 'cold' jets, i.e. jets with total temperature the same throughout, are considered in this study. Only time-averaged flow-field characteristics are addressed. Detailed flow-field data are obtained, mainly through Pitot probe surveys, for various nozzle cases as described in the next section. From data at a given downstream location, the total axial mass flow rate is calculated using procedures and assumptions explained in §2. This quantity, referred to simply as 'mass flux' is used as the primary measure for the comparative study. Although this is an integral quantity, which hides details of the flow field, it provides the most appropriate comparison of the overall entrainment characteristics. Obtaining these data, however, required measurement of the entire flow field in three-dimension space. This was time consuming and had to be carried out gradually as time and facility schedules permitted. This paper is a summary of the results gathered over several years. Most of the results were presented in two earlier conference papers (Zaman 1996*a*; Zaman, Steffen & Reddy 1997). The earlier of the

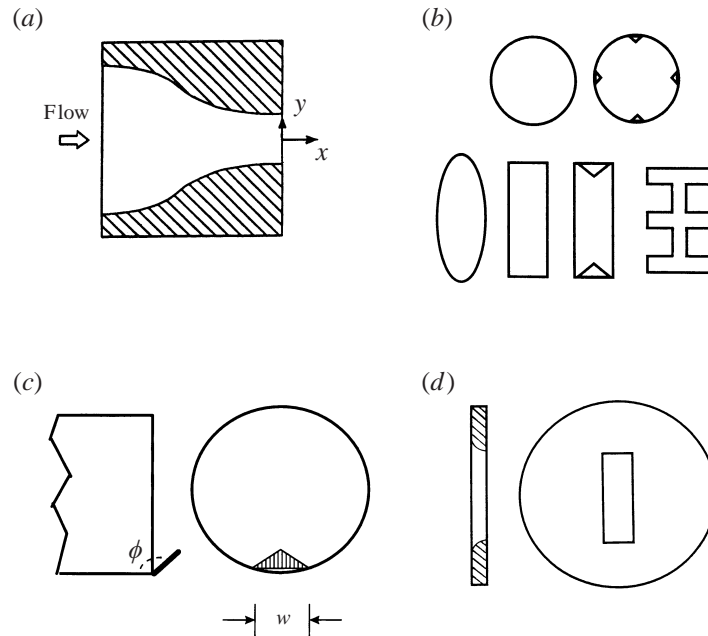


FIGURE 1. Diagram of nozzles, tab configurations, and orifices: (a) nozzle interior shape, (b) nozzle exit geometry with and without tabs, (c) tab geometry, (d) orifice geometry.

two also included data on other details of the flow field, e.g. mode shapes during screeching conditions. The later one had additional computational results on some of the flow fields. Only pertinent elements of those results will be discussed, with the focus on jet spreading. The objective in this overview paper, for the problem at hand with a large parameter space, is to address flow mechanisms causing jet spreading. Specifically, effects of shear layer perimeter stretching, streamwise vortex pairs and unsteady excitation through screech will be compared and evaluated.

## 2. Experimental method

Most of the experiments were carried out in an open jet facility. Compressed air passed through a plenum chamber fitted with flow conditioning units and then exited through the nozzle. The total temperature in the plenum chamber equalled that of the surroundings. The jet discharged in the quiescent air of the laboratory. Further description of the facility can be found in Zaman (1996a,b). For all nozzles, the flow always converged and entered and exited axially (figure 1a). Surveys indicated a top-hat velocity profile at the nozzle exit. Thus, for the present jets, the pressure in the plenum chamber ( $p_t$ ) and the ambient pressure ( $p_a$ ) uniquely defined conditions at the nozzle exit. In the following, the ‘jet Mach number’ ( $M_j$ ) will be used as an independent variable. Even though fictitious in the supersonic regime, its use is common in the literature; it represents the Mach number at the nozzle exit with the flow expanded fully. It is uniquely related to the pressure ratio through the equation,

$$M_j = \left( \left( (p_t/p_a)^{\gamma-1/\gamma} - 1 \right) \frac{2}{\gamma-1} \right)^{1/2},$$

$\gamma$  being the ratio of specific heats.

All asymmetric nozzles were machined from solid cylindrical blocks of aluminium. The interior along the major and the minor axes was contoured according to third-order polynomial fits. The rest of the interior was faired. The asymmetric nozzles included a 3:1 elliptic, a 3:1 rectangular and a 6-lobed case. Mainly two-tab configurations were considered: four equally spaced tabs with the circular nozzle and two large tabs spanning the narrow edges of the 3:1 rectangular nozzle. These are shown in figure 1(b). The equivalent diameter ( $D$ ), based on nozzle exit cross-sectional area, was the same for all asymmetric nozzles, 1.47 cm. The circular nozzle was fabricated earlier, out of clear plastic, and had an exit diameter of 1.27 cm. All nozzles had 'endwalls' to facilitate easy installation of the tabs at desired locations. The tabs used were 'delta-tabs' (Zaman *et al.* 1994), having triangular shapes with the base on the nozzle wall and the apex leaning downstream at about  $\phi = 135^\circ$  (figure 1c); the angle at the apex was about  $90^\circ$ . The width  $w/D$  of the tabs for most of the data with the circular nozzle was 0.28, and that of the tabs with the rectangular nozzle (figure 1b) was 0.53. The geometric area blockage due to each tab was about 2% of the nozzle exit area for the circular case (total blockage about 8%), and about 6% for the rectangular case (total blockage about 12%). The two tab configurations were selected after conducting parametric studies designed to yield a large increase in the jet spreading. A few additional tab cases will be considered in §3.4.3.

In order to carry out a systematic study of the effect of shear layer perimeter stretching, a set of rectangular orifices was fabricated with aspect ratios of 1:1, 2:1, 4:1, 8:1, 16:1 and 32:1, all having the same exit area with an equivalent diameter of 2.54 cm. The orifice geometry is shown schematically in figure 1(d); the entrance was faired with a radius of curvature of about 5 mm, the orifice plate thickness was 6.35 mm.

Hot-wire measurements were performed for the boundary-layer characteristics with the circular nozzle, at low subsonic conditions. The turbulence intensity in the core of the jet was about 0.5%. The momentum thickness variation was found to follow the equation,  $\theta/D = 1.0/(Re_D)^{1/2}$ . However, the fluctuation intensity within the boundary layer was high with a broadband spectrum; thus, the boundary layer was inferred to be 'nominally laminar'. The boundary layer was also measured for a larger, 3:1 rectangular nozzle in connection with the vorticity measurement (§3.4.1). A similar, nominally laminar, boundary-layer state was inferred for that nozzle, with some non-uniformity in the thickness near the corners. Boundary-layer data were not obtained for the other nozzles, since most of the study concerned higher Mach number for which suitable measurement techniques are not available at present. The boundary-layer state for all cases at higher Mach numbers was also most probably 'nominally laminar'. For all cases, including the orifices, Pitot probe surveys at the exit plane indicated 'top hat' velocity distributions.

Most of the flow-field data were obtained by Pitot probe surveys under automated computer control. A rake of three probes was used to reduce data acquisition time. All data were acquired far enough downstream where the flow became fully subsonic in order to avoid measurement errors typical of supersonic flows. The distribution of Pitot pressure, on the cross-sectional plane at a given  $x$ , was integrated to obtain the axial mass flow rate ('mass flux'),  $\dot{m}$ . In the calculation, the static pressure was assumed to be the same as ambient pressure. The integrated flux values were sensitive to small measurement errors, especially at the edges of the flow field, and care had to be taken in the data acquisition. Transducer zero errors were monitored before each run. Throughout data acquisition, the plenum pressure and ambient pressure were

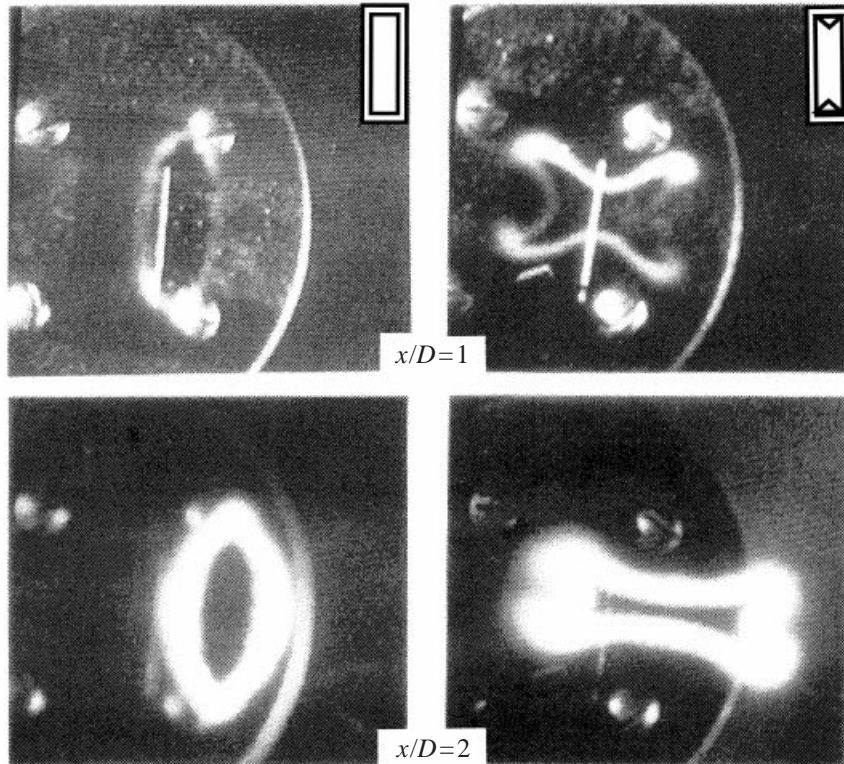


FIGURE 2. Laser-sheet illuminated cross-section of jet from rectangular nozzle with and without tabs:  $M_j = 1.63$ .

monitored and data normalization was carried out according to current conditions. Sufficient averaging time was allowed to ensure good data repeatability.

It should be noted that there is subjectivity in the calculation of the mass flux. Crow & Champagne (1971) had stated, 'The notions of volume flux and entrainment are creatures of theory, in the case of a jet, rather than experiment'. This is because the integrand does not fall off to zero in the surrounding potential flow region and, 'the volume flux in the induced potential flow is infinite'. In all previous experiments, therefore, various criteria were followed to discriminate the vortical flow from the surrounding potential flow. Crow & Champagne did this for their hot-wire data by plotting the integrand, radius times axial velocity, and visually identifying the potential tails of the flux profiles. Note, furthermore, that both hot-wire and Pitot probe measurements involve errors on the periphery of the jet owing to large turbulence and flow angularity. (With a single hot-wire, the measured  $U$ -profile in the potential tail involves slowly diminishing but erroneous positive values primarily due to radial entrainment velocity. In data obtained with a Pitot probe, aligned with the jet axis, small sub-ambient values are erroneously read in the tail region, again, owing to radial entrainment velocity.)

In view of these difficulties, the criterion followed with the present Pitot probe data simply involved truncating the integration where the measured Mach number dropped below 1% of the local centreline Mach number. With the given truncation criterion, care was taken such that most of the data were repeatable within  $\pm 4\%$ ,

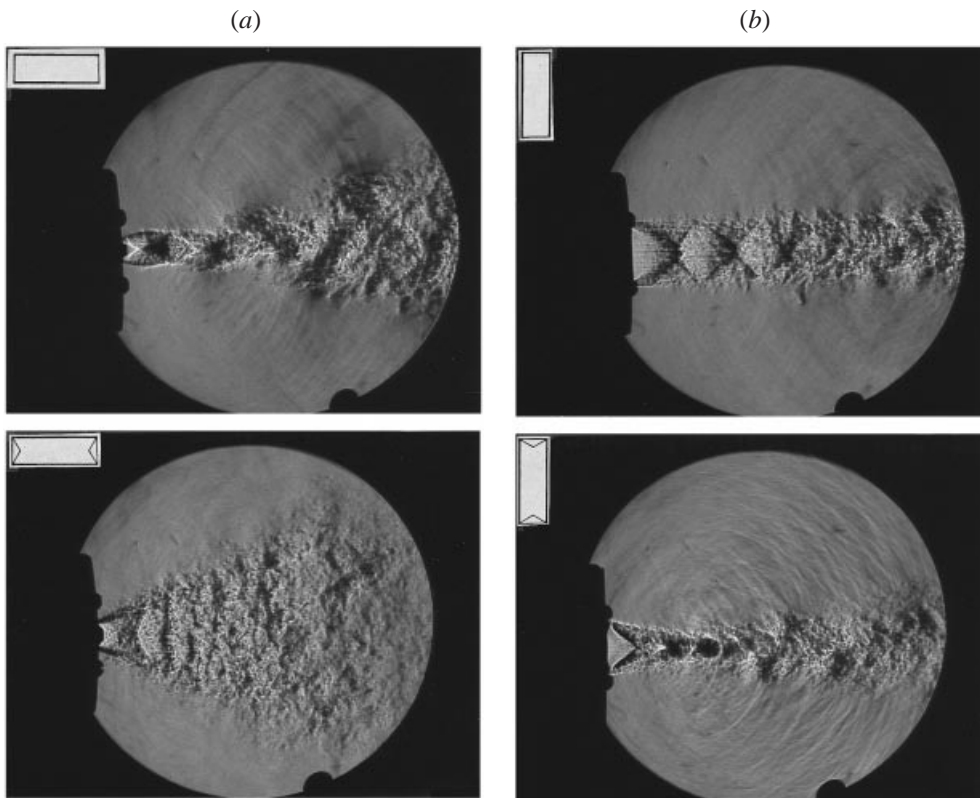


FIGURE 3. Schlieren photograph of jet from rectangular nozzle with and without tabs as indicated;  $M_j = 1.63$ . (a) View of minor axis plane, (b) view of major axis plane.

the repeatability being better at upstream locations where the velocities were higher but worse in cases involving very low jet Mach number.

In addition to the Pitot probe data, streamwise vorticity data obtained by hot-wire anemometry for a low subsonic case will also be presented in comparison to computational results. Distributions of time-averaged transverse velocity components ( $V$  and  $W$ ) were measured on the jet cross-sectional plane using two  $\times$ -wire probes. Gradients of  $V$  and  $W$  yielded the streamwise component of vorticity ( $\omega_x$ ). Further details of the measurement are described by Zaman (1996b). Measurement techniques for some noise and thrust data, also included in the paper, will be discussed with the results. Limited computational results will be presented in order to augment and reinforce some of the inferences. The computational procedure will be briefly described along with the results in § 3.4.1.

### 3. Results

Examples of flow-visualization pictures are shown in figures 2–4 to illustrate, especially, the impact of the tabs on jet spreading. In figure 2, laser-sheet illuminated cross-sections of the rectangular jet are shown with and without tabs. The visualization is carried out, without any artificial seeding of the flow, by simply shining the laser-sheet across the jet. Moisture from entrained ambient air condenses when coming in contact with the low-temperature air in the core of the supersonic jet. The laser-sheet

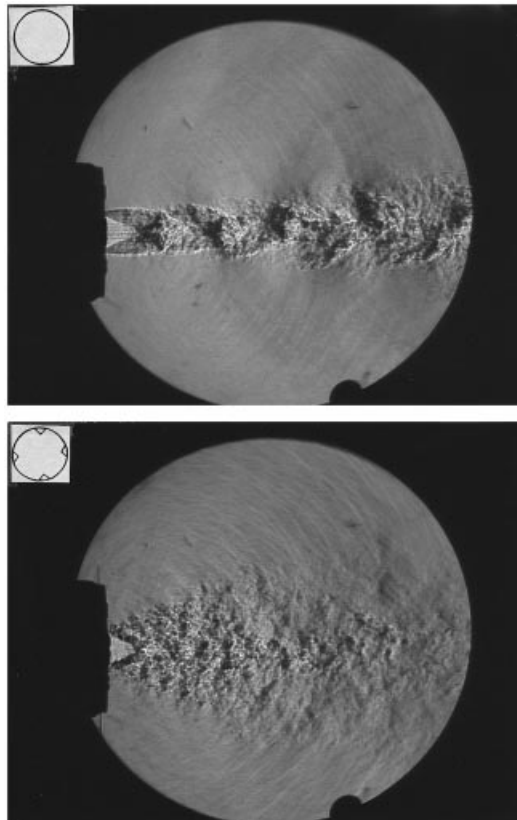


FIGURE 4. Schlieren photograph of jet from circular nozzle with and without tabs:  $M_j = 1.63$ .

illuminates the condensed moisture particles, and, thus, essentially the mixing-layer region. The nozzle major axis is vertical in these pictures, and an evolution of the jet cross-section into an oval shape can be seen for the no-tab case. The pronounced effect of the tabs can be seen easily. At  $x/D = 1$ , the mixing layer has already curled up in the lateral direction. By  $x/D = 2$ , the jet cross-section has elongated significantly in the direction of the minor axis of the nozzle, i.e. 'axis switching' has already taken place (Zaman 1996*b*). As will become clear later, the axis switching also occurs with the no-tab case, but farther downstream, at this supersonic condition.

Schlieren photographs of the flow field are shown in figures 3(*a*) and 3(*b*) for the rectangular nozzle with and without tabs. Figure 3(*a*) shows the views on the minor axis plane of the nozzle. The picture at the bottom of figure 3(*a*) vividly illustrates the increase in the overall jet spreading caused by the tabs. The shock/expansion structures are weakened drastically by the tabs. The overall increase in spreading is also accompanied by an increase in small-scale mixing, as apparent from the 'graininess' of the pictures. (Note that these are instantaneous pictures of the flow field whereas the pictures in figure 2 were time-averaged.) Since the jet goes through a rapid axis switching in this case, the spreading is not as much on the major axis plane (figure 3*b*). Initially, there is actually a decrease in the jet width on this plane relative to the no-tab case. However, by the farthest downstream region on the right-hand side, the width has become more than that of the no-tab case. Corresponding pictures for the circular nozzle, with and without tabs, are shown in figure 4. The spreading

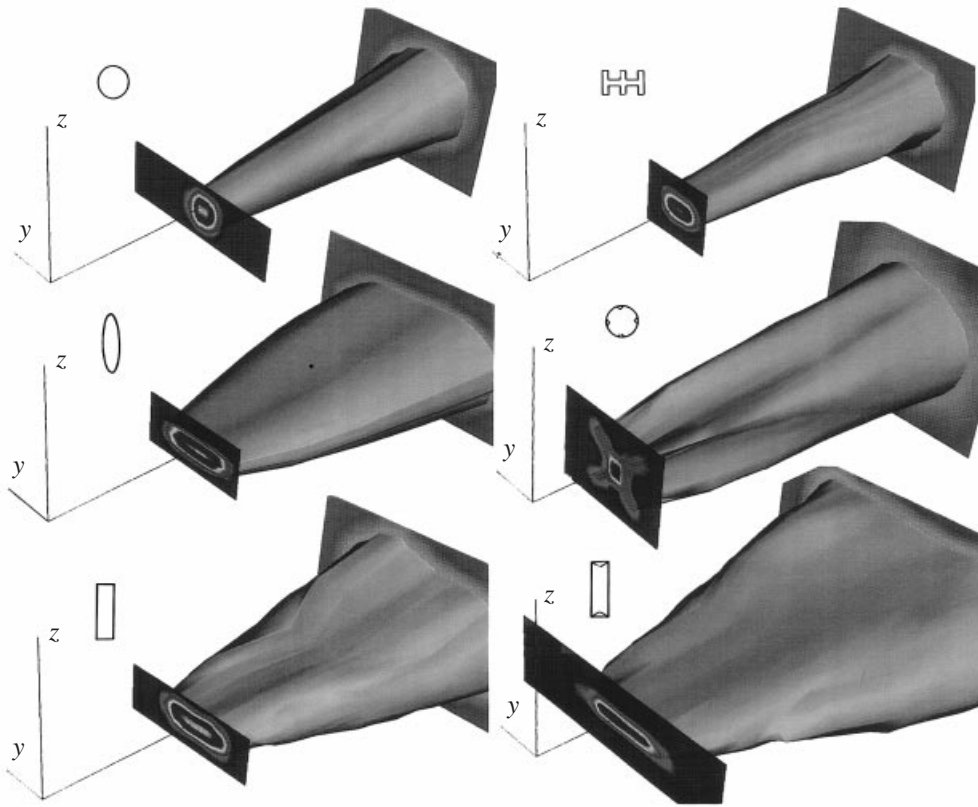


FIGURE 5. For  $M_j=1.63$ , iso-surfaces of Mach number,  $M/M_{MAX} = 0.3$ , for the six nozzle cases of figure 1(b);  $M_{MAX}$  is maximum Mach number at a given  $x$ . Data cover  $x/D$  range of 10–30 for the no-tab cases and 5–30 for the tab cases.

caused by the tabs, although not as much as seen in figure 3(a), is still quite significant. The spreading is relatively uniform in the azimuthal direction in this case.

From the Pitot probe surveys, overall flow-field evolution is constructed for the six nozzle cases of figure 1(b). This is shown by an iso-surface of the normalized velocity, in figure 5 for  $M_j = 1.63$ , and, in figure 6 for  $M_j = 0.3$ . For the rectangular and elliptic cases without tabs, at the supersonic condition (figure 5), an axis switching can be seen to have taken place by the first measurement station ( $x/D = 10$ ). (The nozzle major axis is aligned with the  $z$ -direction.) There is, however, no axis switching apparent in the corresponding flows at the subsonic condition (figure 6). It is also clear that, with the case of the rectangular nozzle with tabs, there is a pronounced axis switching at both Mach numbers. This is also the case that exhibits the most overall spreading. The lobed nozzle case, on the other hand, especially at the supersonic condition (figure 5), does not exhibit an increased spreading. These effects are quantified by the mass flux data in the following.

Normalized mass flux variations with streamwise distance for a low subsonic Mach number are shown in figure 7(a). As expected, the fluxes for the circular jet are found to be the smallest at all  $x$ . Corresponding fluxes for the elliptic, rectangular and lobed cases are somewhat higher. However, they are not as high as reported in some earlier studies. In Ho & Gutmark's (1987) work, for example, the mass flux measured at  $x/D = 5$  for a 2:1 elliptic jet was about 55% higher than that for a circular jet. The



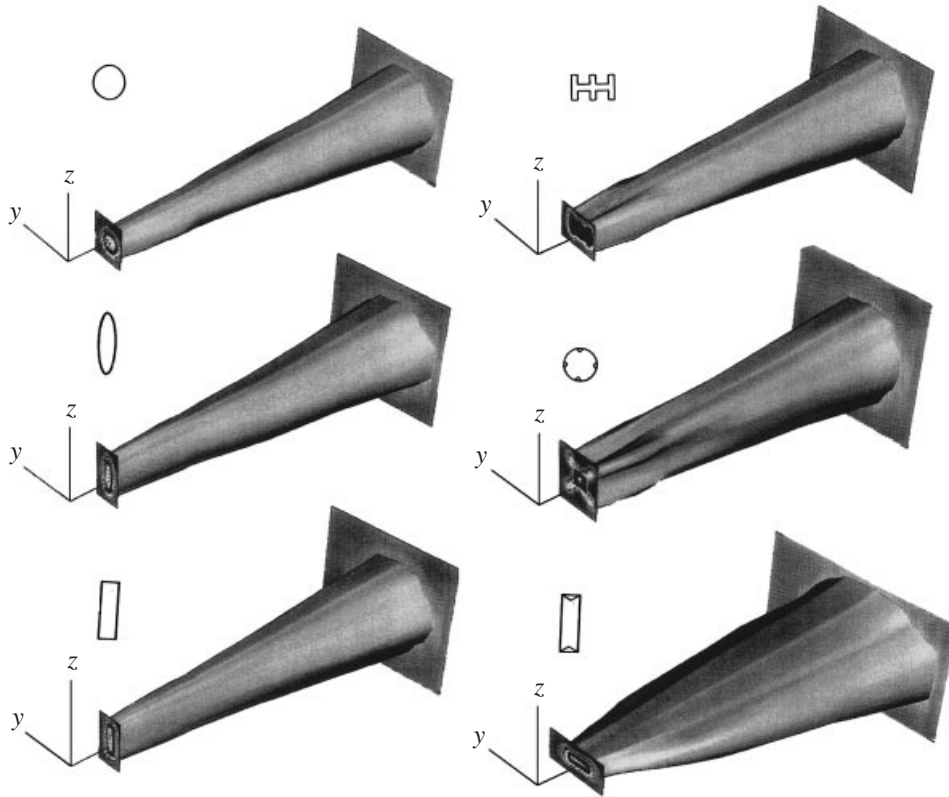


FIGURE 6. For  $M_j = 0.3$ , iso-surfaces of mean velocity,  $U/U_{MAX} = 0.3$ , for the six nozzle cases;  $U_{MAX}$  is maximum velocity at a given  $x$ . Data cover  $x/D$  range of 2–19.

corresponding increases for the elliptic and the rectangular jets in figure 7(a) are less than 10%. A possible reason for this difference is discussed in §3.3.

Referring back to figure 6, the cross-sections of all the jets, except the rectangular one with tabs, can be seen to have become essentially round by the farthest downstream location. These jets have apparently reached the asymptotic, self-similar state and, thus, the entrainment rates, given by the slopes of the flux curves, are comparable. The rate,  $\partial(\dot{m}/\dot{m}_e)/\partial(x/D)$ , based on the farthest two data points in figure 7(a), turns out to be about 0.28. This is in reasonable agreement with previous round-jet data (Ricou & Spalding 1961; Crow & Champagne 1971; Zaman 1986). For the rectangular jet with tabs, the jet cross-section remains non-circular within the measurement range. Thus, this jet is still evolving, presumably tending to attain a circular cross-section, and the process is accompanied by a higher entrainment rate. For the two tab cases, mass flow rate,  $\dot{m}_e$ , for data normalization, was measured by an upstream orifice meter. This measurement was not made when presenting the flux data in the two earlier conference papers, Zaman (1996a) and Zaman *et al.* (1997). There,  $\dot{m}_e$  was calculated assuming uniform flow and by accounting for the geometric area blockage. This explains a slight difference in the normalized flux values for the tab cases presented here and in those two papers. The geometric and actual flow blockages are discussed in §3.4.3.

The mass flux data for a high subsonic Mach number (0.95) are shown in figure 7(b).

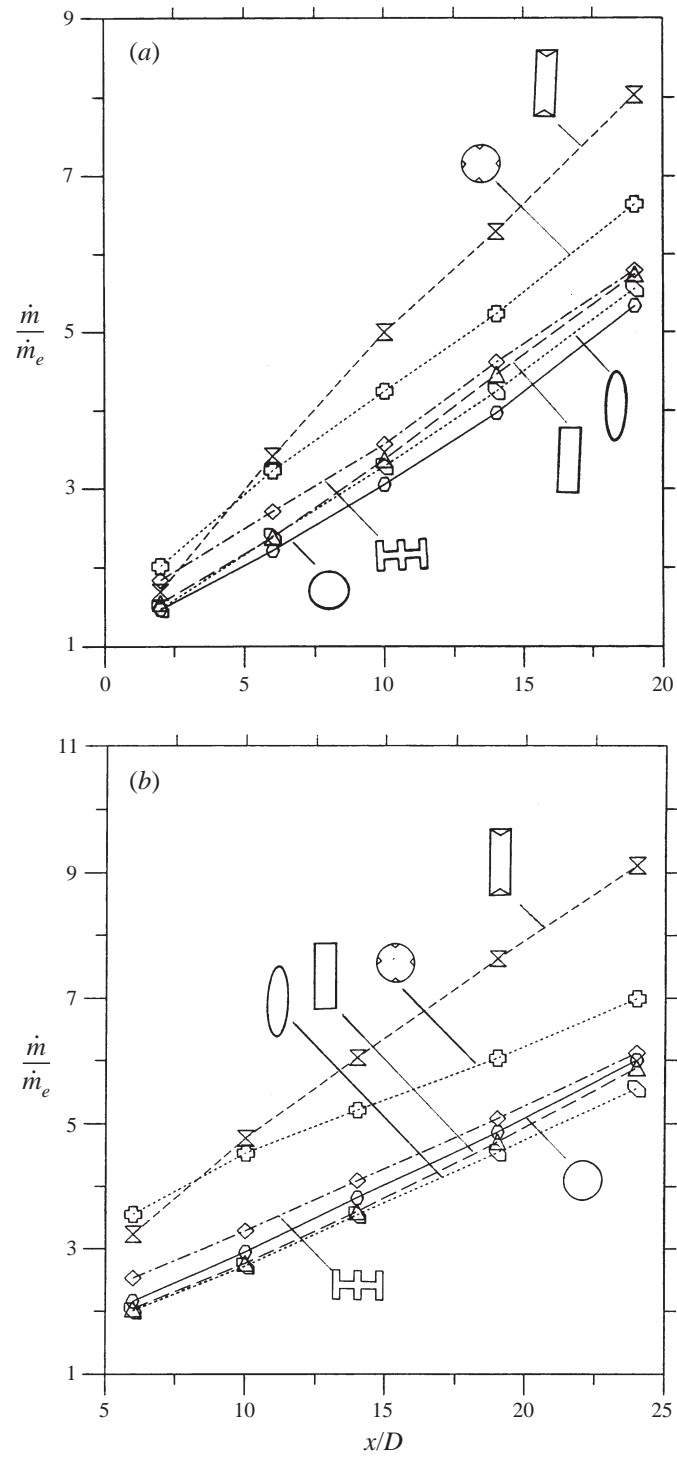


FIGURE 7 (a, b). For caption see facing page.

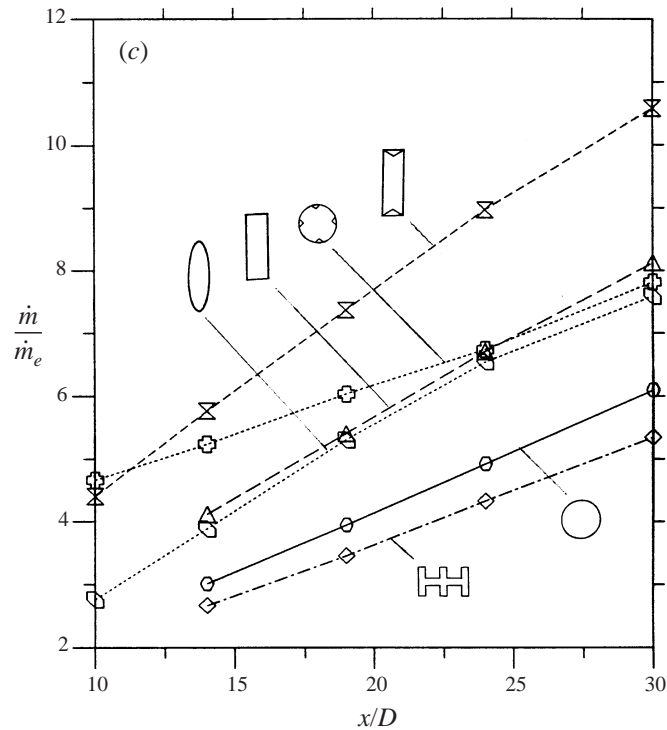


FIGURE 7. Streamwise variation of normalized mass flux for the six nozzle cases:  
 (a)  $M_j = 0.3$ , (b)  $M_j = 0.95$ , (c)  $M_j = 1.63$ .

Essentially similar trends, as with the low subsonic condition, are observed. There are changes in the slopes with increasing compressibility, and this will become clearer with data for the supersonic case. Somewhat surprisingly, the flux amplitude for the circular jet is found to be consistently higher than that of the rectangular and elliptic jets. The reason for this is not clear. It is conjectured that, because the exit edge of the circular nozzle (made out of clear plastic) was slightly rounded, an unsteady normal shock existed at this Mach number which might have caused an 'excitation' leading to an increased spreading.

The mass flux data for the supersonic condition are presented in figure 7(c). A few observations can be made. First, the curve for the circular jet is found to have attained a constant slope, the rate being about 0.18. This is much lower than that observed at the subsonic conditions. Secondly, the mass flux values for the lobed nozzle are found to be even lower than that for the circular nozzle. Thirdly, the fluxes of both the elliptic and the rectangular jets are found to be significantly higher than that of the circular jet. This is in contrast to the subsonic condition where the corresponding difference was smaller. Fourthly, the circular jet with four tabs exhibits a much higher flux in the upstream region, indicating that a more vigorous entrainment process occurred farther upstream. Towards the end of the measurement range, however, the jet cross-section in this case has become approximately round and the slope of the flux curve has become comparable to that of the corresponding no-tab case. Finally, as with the subsonic cases, the rectangular jet with two tabs is found to involve the most vigorous entrainment within the measurement range. The observations listed in this paragraph will serve as the basis for further discussion in the following.

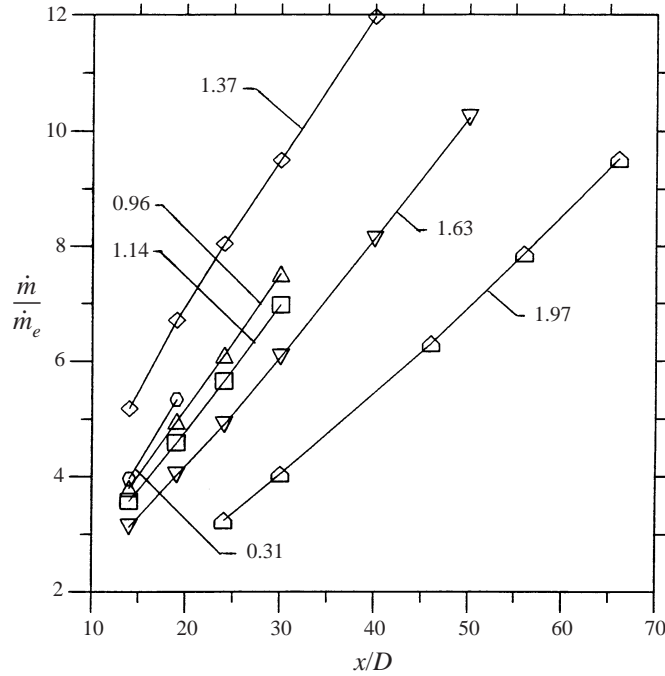


FIGURE 8. Streamwise variation of normalized mass flux for indicated  $M_j$ , circular nozzle.

### 3.1. Asymptotic entrainment rate for initially compressible jets

The slopes of the mass flux curves for the circular jet in the far downstream regions are found to decrease with increasing Mach number,  $M_j$ . These slopes, from figures 7(a)–7(c), are 0.28, 0.24 and 0.18 for  $M_j = 0.3$ , 0.95 and 1.63, respectively. A similar effect is also observed for the other nozzles for which the jet cross-section has become round.

This effect was studied further with the circular nozzle. Mass flux curves for additional jet Mach numbers are shown in figure 8. With increasing  $M_j$  the measurements had to be carried out farther downstream until the streamwise variation was deemed linear. In this section, the asymptotic spreading rates, determined from the slopes of the curves measured in the farthest downstream regions, are considered. These slopes, ( $K = \partial(\dot{m}/\dot{m}_e)/\partial(x/D)$ ), are plotted in figure 9(a) as a function of  $M_j$ . The decrease in the asymptotic spreading rate with increasing  $M_j$  is clearly shown by these data.

Dimensional analysis would indicate that the asymptotic spreading rate should scale as the square-root of the ratio of densities at the nozzle exit and in the surroundings (Ricou & Spalding 1961; Witze 1974). Thus, when normalized by  $(\rho_a/\rho_e)^{1/2}$  the rate might be expected to become a constant and independent of  $M_j$ . This is examined in figure 9(b) where the same data as in figure 9(a) are replotted with such normalization. It is found that the normalized slope is not a constant and varies across the transonic region. These trends can be explained as follows.

For the asymptotic region, dimensional analysis provides:

$$\dot{m} = K_1 \dot{F}^{1/2} \rho_a^{1/2} x, \quad (1)$$

where  $\dot{F}$  is the momentum flux in the asymptotic region,  $\rho_a$  is the ambient air density,  $x$  is the distance from the nozzle (large compared to  $D$ ), and  $K_1$  is a constant. With

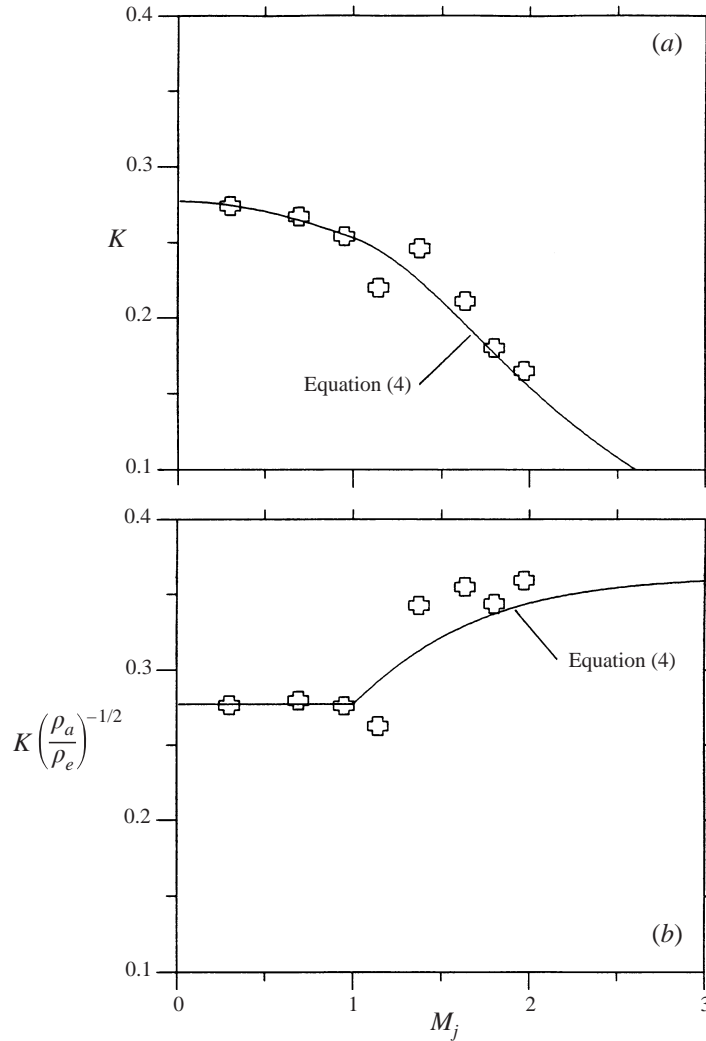


FIGURE 9. Asymptotic slope,  $K = \partial(\dot{m}/\dot{m}_e)/\partial(x/D)$ , for the circular nozzle; the solid line represents equation (4). (a) Slopes as measured, (b) normalized slopes.

an appropriate control volume,  $\dot{F}$  can be equated with forces at the nozzle exit as,

$$\dot{F} = A_e \rho_e U_e^2 + (p_e - p_a) A_e, \quad (2)$$

where the subscript  $e$  denotes conditions at the nozzle exit,  $A_e$  being the nozzle exit area. Let  $\dot{F} = \xi A_e \rho_e U_e^2$ , so that,

$$\xi = 1 + (p_e - p_a) / \rho_e U_e^2. \quad (3)$$

Substituting in (1), with  $\dot{m}_e = A_e \rho_e U_e$ , it follows that  $\dot{m}/\dot{m}_e = K_1 \xi^{1/2} (A_e \rho_e U_e^2)^{1/2} \rho_a^{1/2} x / (A_e \rho_e U_e)$ . With  $A_e = \frac{1}{4} \pi D^2$  and  $K_2 = K_1 (4/\pi)^{1/2}$ , it follows that,

$$\frac{\dot{m}}{\dot{m}_e} = K_2 \xi^{1/2} \left(\frac{\rho_a}{\rho_e}\right)^{1/2} \left(\frac{x}{D}\right). \quad (4)$$

The coefficient on the right-hand side of equation (4), ( $K = K_2 \xi^{1/2} (\rho_a/\rho_e)^{1/2}$ ), is assumed to be equal to 0.28 for incompressible jets (as discussed before). For compressible jets,  $\xi$  and  $\rho_e$  must be calculated so that the variations of  $K$  with  $M_j$  can be predicted.

Through the subsonic regime ( $M_j \leq 1$ ),  $p_e = p_a$ , therefore,  $\xi = 1$  (3). As the flow enters the (underexpanded) supersonic regime with increasing nozzle pressure ratio  $p_t/p_a$  (and hence  $M_j$ ), one-dimensional nozzle flow analysis would predict a discontinuity in the variation of  $p_e$ , and hence in  $\xi$ . In the supersonic regime, the Mach number at the nozzle exit is unity (i.e. design Mach number  $M_D = 1$ ), and  $p_e$  is given by,  $p_e/p_t = (1 + \frac{1}{2}(\gamma - 1)M_D^2)^{-(\gamma/\gamma-1)}$ . Since  $U_e = M_D(\gamma RT_e)^{1/2}$ , (3) provides,

$$\xi = 1 + \frac{1}{\gamma M_D^2} (1 - p_a/p_e). \quad (5)$$

From these expressions,  $\xi$  can be found at any  $p_t/p_a$ . Similarly, the density at the nozzle exit,  $\rho_e$ , can be calculated. In the subsonic regime, the Mach number at the nozzle exit is,

$$M_e = \left( \left( (p_t/p_a)^{\gamma-1/\gamma} - 1 \right) \frac{2}{\gamma-1} \right)^{1/2},$$

and in the supersonic regime  $M_e = M_D = 1$ . The density,  $\rho_e$  is then given by,

$$\rho_e/\rho_t = \left( 1 + \frac{1}{2}(\gamma-1)M_e^2 \right)^{-1/\gamma-1},$$

where  $\rho_t = p_t/RT_t$ . These calculations are performed to obtain the analytical curves from (4) which are shown in figures 9(a) and 9(b). The value of the slope has been matched on the left-hand end with  $K = 0.28$ . As stated earlier, this is the approximate value of the slope observed in previous experiments. This is the only matching that has been carried out in the analysis, the rest following from compressible flow equations. The agreement with the data can be seen to be quite good.

Inspecting (4) and (5), it should be clear that the value of the slope,  $K(\rho_a/\rho_e)^{-1/2} = K_2 \xi^{1/2}$ , should be 0.28 up to  $M_j = 1$ . At large  $M_j$ , with  $\gamma = 1.4$  for air, it should reach an asymptotic value of 0.367. This trend is approximately followed in figure 9(b). The reason why normalization by  $(\rho_a/\rho_e)^{1/2}$  does not yield a constant value of the slope (i.e. constant value of  $K(\rho_a/\rho_e)^{-1/2}$  can be traced to the appearance of the pressure term in the momentum balance equation(2). This leads to the observed jump in the slope across the transonic region.

In passing, it should be noted that the assumption that  $p_e = p_a$  in the subsonic regime does not strictly hold even for incompressible flows (see e.g. Hussain & Clark 1977). However, the effect of the deviations in  $p_e$  for that regime is already included in the incompressible constant ( $K = 0.28$ ) assumed in the analysis. This section is concluded by noting that the observed trend in figure 9(a) is simply a consequence of the usual (and most practical) choice of parameters for data normalization, based on conditions at the nozzle exit. The decrease in the slope is not due to the well-known compressibility effect that causes a decrease in mixing with increasing Mach number (Papamoschou & Roshko 1988; Samimy & Elliot 1990). The observed decrease is entirely due to variations in density and static pressure at the nozzle exit, as the analysis has demonstrated. A further analysis of these effects, with additional data from a convergent-divergent nozzle, will be presented separately.

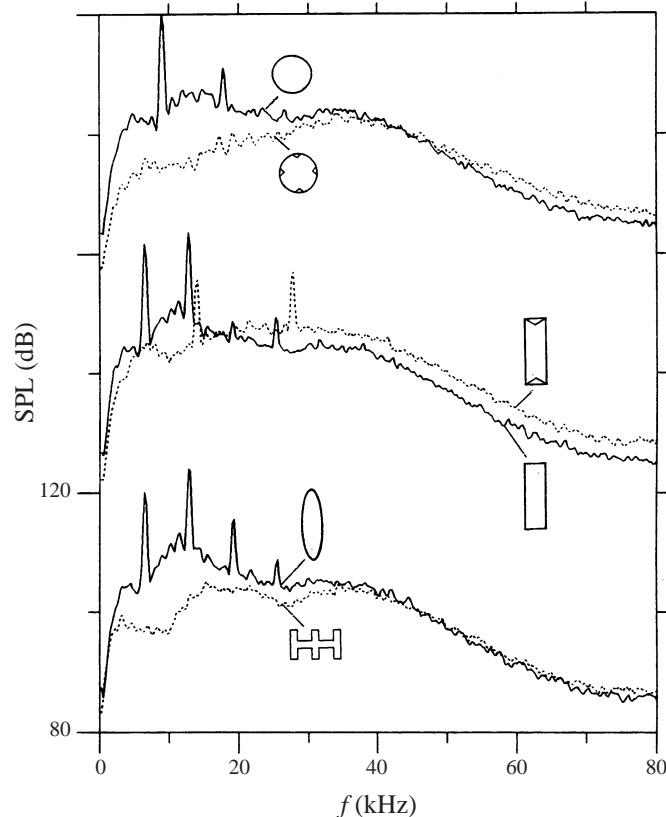


FIGURE 10. Far-field noise spectra for the six nozzle cases at  $M_j = 1.63$ ; the three pairs of traces are staggered successively by one major ordinate division.

### 3.2. Effect of screech on jet spreading

The second point made with figure 7(c) was that the least amount of spreading occurred with the lobed nozzle. Owing to the stretching of the perimeter of the shear layer, more mixing and entrainment is expected with a lobed nozzle. Thus, the result that the lobed nozzle produced even less jet spreading than the circular nozzle came as a surprise. Soon the reason became apparent. At  $M_j = 1.63$ , all jets (without tabs) involved screech, whereas there was no screech with the lobed nozzle. It may be reasoned that the presence of screech with the other nozzles, and the absence thereof with the lobed nozzle, caused the difference.

First, far-field noise spectra for the six nozzle cases are shown in figure 10. These data were obtained with a  $\frac{1}{4}$ -inch (B&K) microphone located approximately  $70D$  away from the jet axis and about  $110^\circ$  from the downstream axis. For ease of comparison, the data are shown in three pairs. The fundamental screech component at about 9 kHz can be clearly seen for the circular jet. This is, eliminated when the tabs are applied. Both the rectangular and the elliptic nozzles are also characterized by screech noise. Use of the tabs does not completely eliminate screech from the rectangular nozzle but the amplitudes are reduced drastically together with a shift in the frequencies. It is also clear that the lobed nozzle does not involve any screech noise. This is generally true throughout the jet Mach number range covered in the study.

Screech is a phenomenon that occurs in imperfectly expanded supersonic jets owing

to the interaction of coherent azimuthal vortical structures with the standing shock-expansion cells (see e.g. Powell 1953; Tam 1991). The vortical structures are organized and rendered periodic through a feed-back loop, with a resultant emission of a tone 'of definite frequency and high intensity' (Davis & Oldfield 1962).

Screech is also accompanied by an increase in jet spreading. The first known investigation addressing this effect for a circular jet is that of Glass (1968). The generation of screech in Glass's study caused a 'precipitous drop' in the 'impact pressure' measured on the jet axis, clearly indicating an increase in the spreading of the jet. This was further investigated by Sherman, Glass & Duleep (1976), and, for a rectangular jet, by Krothapalli *et al.* (1986), leading to similar conclusions that jet spreading increased in the presence of screech.

Based on past studies on the effect of artificial excitation on incompressible jets, the following comments can be made on the likely mechanism for the observed impact of screech on jet spreading. The effect of artificial excitation, when imparted at an appropriate frequency, is to organize (i.e. reduce randomness and make periodic) and intensify (i.e. concentrate into tighter cores) the coherent vortical structures. These are the unsteady, azimuthal vortical structures; in the case of a circular jet, these are typically toroidal structures that roll-up periodically under the excitation. These structures evolve, azimuthal distortion develops and interactions among adjacent structures take place, as they convect downstream. The toroidal structures break down into disorganization near the end of the potential core as the mean velocity profile transitions into a fully developed shape. The process is usually accompanied by an increase in entrainment. For example, in the work of Crow & Champagne (1971) an increase in the entrainment of a circular jet was observed under acoustic excitation at the 'preferred mode' Strouhal number. About a 15% increase in the volume flux was measured in the  $x/D$  range of 8–10. The additional entrainment occurred mostly near the end of the potential core ( $x/D \approx 4$ ) where the intensified vortical structures started to break down. It is the organization and intensification and the subsequent dynamics of the coherent structures, under screeching condition, that are also believed to lead to the increased jet spreading.

The higher entrainment with the elliptic and rectangular jets at the supersonic condition, compared to that at the subsonic condition (the third observation made with figure 7), is also believed to be due to screech. Periodic excitation can have a more profound impact on an asymmetric jet compared to that on an axisymmetric jet. In the work of Hussain & Husain (1989), acoustic excitation of elliptic jets has been shown to cause a dramatic increase in the jet spreading. A similar observation is made for a rectangular jet by Zaman (1996*b*). In these cases, the azimuthal vortical structures, organized and intensified under the excitation, are initially asymmetric in shape. Such asymmetric vortical structures go through a sequence of contortion owing to self-induction which not only cause axis switching (Hussain & Husain 1989; Ho & Gutmark 1987; Zaman 1996*b*), but also result in an increased entrainment. Again, it is thought that a similar mechanism is at play with the asymmetric jets when screech occurs. This is, at least, partially responsible for the larger increase in the fluxes at the supersonic condition (figure 7*c*) compared to the increase at the subsonic condition (figure 7*a*). This also explains the axis switching seen in the supersonic cases (figure 5) which did not occur in the subsonic cases (figure 6).

The discussion so far in this section has been based on previous studies involving 'plane wave' excitation. Jet excitation has been studied with more complex waveforms (helical mode, combination of modes, subharmonic resonance, etc.). In most cases, excitation at the other modes also causes an increase in jet spreading (Parekh,



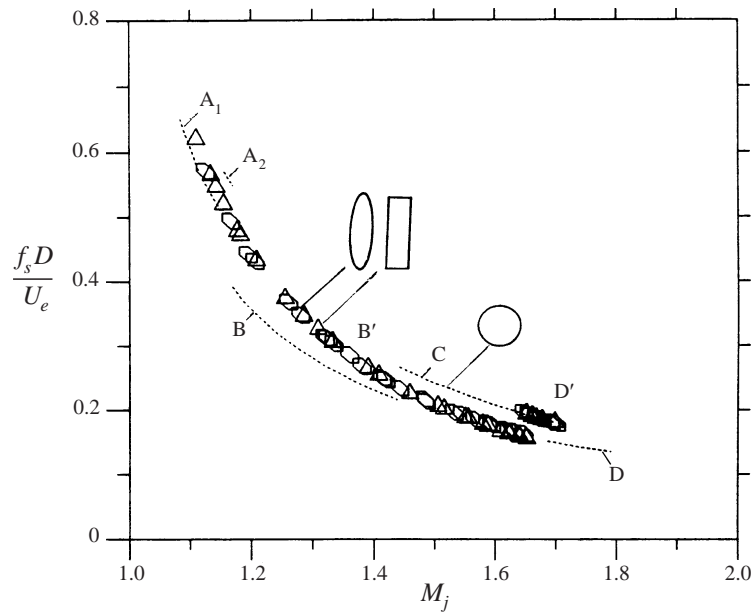


FIGURE 11. Non-dimensional screech frequency ( $f_s$ ) versus  $M_j$  for the indicated nozzles; letters indicate screech stages.

Reynolds & Mungal 1987; Raman, Rice & Reshotko 1991). Screech involves self-excitation in a variety of modes. The characteristics of these modes and their impact on jet spreading are further discussed in the following.

### 3.2.1. Unsteady flow characteristics in various modes of screech

The variation of screech frequency, expressed as Strouhal number based on the equivalent diameter, for the circular, elliptic and rectangular nozzles is shown in figure 11. Here,  $f_s$  is the screech frequency and  $U_e$  is the velocity at the jet exit. The triangular and 'elliptical' symbols represent the rectangular and elliptic jets, respectively, whereas the dotted lines represent data for the circular jet. It is well known that screech for the circular nozzle goes through different 'stages', involving different modes of unsteady flow oscillation, as  $M_j$  is varied. These involve flow-field oscillations in the axisymmetric (stages  $A_1$  and  $A_2$ ), flapping (B and D) and helical (C) modes. For proof and discussion of the mode shapes occurring with a circular nozzle, see, e.g. Powell, Umeda & Ishii (1990); Norum (1983); Ponton & Seiner (1995); and Panda (1995). Zaman (1996a) provided additional data and a summary of the past work. It should be added here that although the B mode primarily involves a flapping motion, it is unstable and has been observed to switch between helical and flapping motions (Ponton & Seiner 1995).

Corresponding frequency characteristics for the rectangular and the elliptic jets also exhibit a staging behaviour involving one frequency jump within the measurement range. This can be seen in figure 11. There are two stages and these are denoted by the primed letters. A jump occurs from the B' stage to the D' stage around  $M_j = 1.65$  ( $p_t/p_a = 4.61$ ), with a certain amount of overlap, for both nozzles. It was determined from unsteady pressure field surveys that both the B' and D' stages involved flapping mode oscillation, the flapping occurring about the major axis plane. These data have been presented in Zaman 1996a, and are not repeated here.

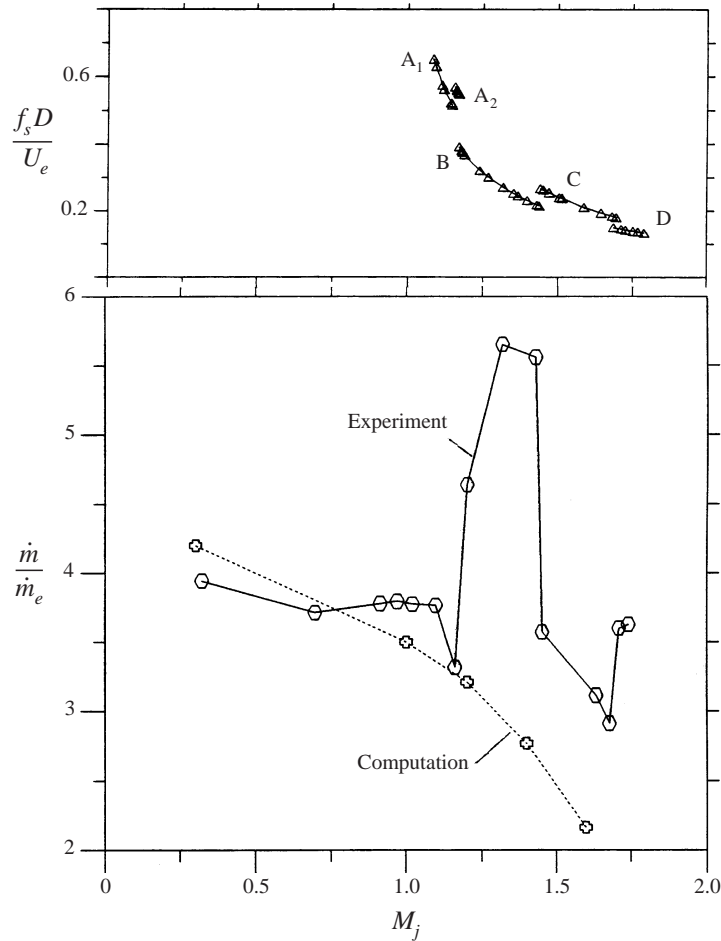


FIGURE 12. Normalized mass flux, at  $x/D = 14$ , versus  $M_j$  for the circular nozzle. Non-dimensional screech frequency is shown on the top.

Why does the jet go through a frequency jump from stage B' to D' with seemingly similar unsteady motion? Why does the circular jet go through a jump from the A<sub>1</sub> to A<sub>2</sub> stage with both having axisymmetric unsteady motion? What dictates the other modal structures with the circular nozzle? What chooses the direction of the helical motion as well as the plane about which the flapping motion occurs? These issues, and the complete mechanism for the screech noise generation, have remained far from clear and are beyond the scope of the present work. Here, we turn attention to the effect of these screech modes on jet spreading.

### 3.2.2. Effect of various screech modes in jet spreading

The normalized mass flux variation, measured at a fixed downstream location ( $x/D = 14$ ), with  $M_j$  for the circular jet is shown in figure 12. The corresponding screech stages (figure 11) are reproduced on the top for comparison. The fluxes undergo large variation with  $M_j$ . The fluxes are highest in the flapping mode B, and are again relatively high in the next flapping mode D. With the onset of the helical mode C, the flux values drop substantially. It should be noted that screech amplitude (but not the frequency and mode shape) has been known to be sensitive to the details

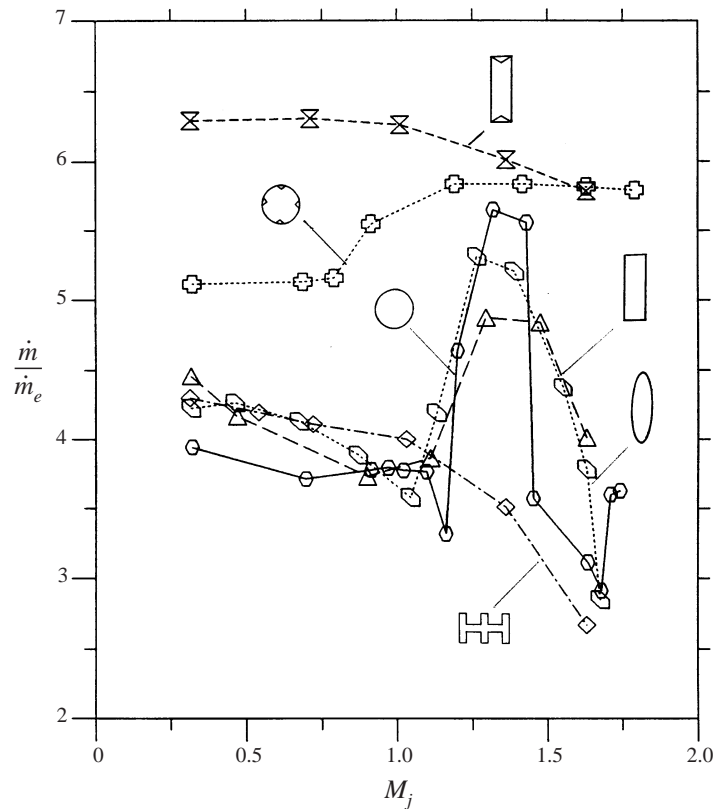


FIGURE 13. Normalized mass flux at  $x/D=14$  versus  $M_j$  for the six nozzle cases.

of the nozzle geometry such as the lip thickness. The screech amplitude is likely to affect the flux values. Thus, with a different nozzle the flux amplitudes may not be repeatable but the trend with varying screech stages may be expected to remain the same. Thus, the present results are in agreement with the Pitot probe data obtained, at a single point on the jet centreline, by Glass (1968) and Sherman *et al.* (1976). For example, the drop in the total pressure was observed in those studies to be the most at pressure ratios corresponding to the B mode indicating the largest increase in jet spreading.

It is reasonable to infer that had there been no screech, the flux values in figure 12, in the supersonic regime, would be lower. The steady-state computational results, included in figure 12, provide an idea about the expected trend had there been no screech. (These computations were performed as part of the effort towards resolving the flow field of the tabbed jets; see §3.4.1 and Steffen, Reddy & Zaman (1997). Questions remain regarding the effect of turbulence model and the computational procedures on the fidelity of the results. These aspects have also been discussed by Reddy, Steffen & Zaman (1997).) However, it is clear that the occurrence of screech generally increases jet spreading, and this effect is most pronounced in the flapping modes. Referring back to figure 7(c), note that the data for the circular jet (at  $M_j = 1.63$ ) involved screech in the C mode that is characterized by relatively smaller flux amplitudes. Therefore, the difference between the circular and the lobed nozzle

data would have been more dramatic at either a lower or a higher  $M_j$  yielding the B or D screech modes for the circular nozzle.

Corresponding mass flux data, obtained at  $x/D = 14$ , for all six nozzle cases are compared in figure 13. The fluxes for the elliptic and the rectangular jets are clearly high in the B' mode. The pattern is similar to the circular jet B' mode. The flux values drop as the D' mode is approached. It is possible that the screech amplitude, which diminishes as a stage jump is approached, is responsible for the trend. In general, however, it is clear that the flapping mode screech results in the highest jet spreading. Note that the flapping mode can result from a superposition of two opposite sign helical modes. The observed effect is generally consistent with artificial excitation studies for circular jets in which multiple modes of excitation were employed (Strange & Crighton 1983; Cohen & Wygnanski 1987; Parekh *et al.* 1987). Referring back to figure 7(c) and the discussion earlier in this section, an additional, perhaps the main reason for the relatively higher fluxes with the asymmetric jets becomes clear. At  $M_j = 1.63$ , the elliptic and the rectangular jets went through a flapping mode screech, whereas the circular jet went through a helical mode screech. The difference in screech mode contributed to the higher fluxes observed for the asymmetric jets.

Let us note that the fluxes for the tab cases in figure 13 are much larger throughout the jet Mach number range. The values are larger than those obtained with any of the asymmetric nozzles. This is true for supersonic as well as subsonic conditions. Note especially that the circular jet with tabs does not involve screech. Whereas the spreading increase with screech occurs through an organization of the azimuthal vortical structures and their subsequent dynamics, that with the tabs occurs primarily through the dynamics of the streamwise vortex pairs. This is discussed further in § 3.4.

### 3.3. Effect of shear layer perimeter stretching on jet spreading

The result that the asymmetric nozzles produced only marginal increase in the fluxes relative to the circular case even at subsonic conditions was also surprising. As stated before, an underlying concept with an asymmetric (e.g. lobed) nozzle is to stretch the perimeter of the shear layer that increases the interfacial area between the high- and low-speed streams. This is expected to increase mixing. Yet, the increase in the fluxes with all asymmetric nozzles (figure 7a,b) was marginal. The results with the elliptic and rectangular nozzles contrasted previous observations by others (Ho & Gutmark 1987; Hussain & Husain 1989). This prompted further investigation.

A simple way to stretch the mixing layer would be to increase the aspect ratio ( $AR$ ) of a rectangular nozzle while keeping the exit area the same. This was done with the orifice cases as described earlier. An advantage of using the orifices, instead of nozzles, was that streamwise vorticity due to upstream secondary flow should be minimal, thus, jet spreading due simply to the shear layer perimeter stretching could be studied.

The mass flux variations obtained with the orifices, at  $M_j = 0.95$ , are shown in figure 14. It can be seen that for  $AR$  up to 8:1, the jet spreading has essentially remained the same and is basically indistinguishable from the data obtained with the circular nozzle. Only when  $AR$  is increased to 16, does an increase in the jet spreading finally occur. As expected, the effect becomes clearly pronounced with even larger  $AR$  (32:1). (In the limit of aspect ratio tending to infinity, the initial slope of the flux curve, with the given coordinates, should also tend to infinity.)

The present data suggest that the effect of shear layer perimeter stretching on the spreading of a rectangular jet becomes significant only when the aspect ratio is very large. We note here that the 6-lobed nozzle (figure 1b) has a wetted perimeter

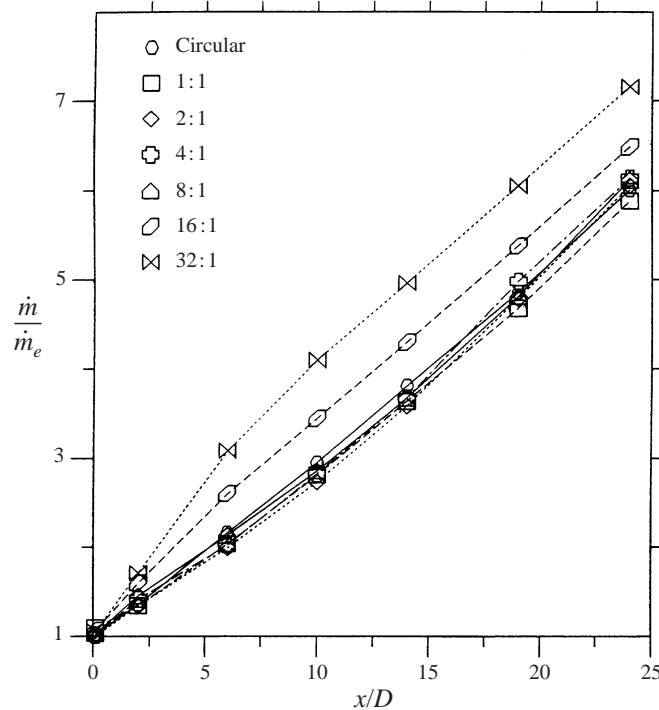


FIGURE 14. For  $M_j = 0.95$ , streamwise variation of normalized mass flux for the rectangular orifice cases with indicated aspect ratios; 'circular' represents circular nozzle data from figure 7(b).

equivalent to a rectangular nozzle of  $AR$  of about 16. The spreading increase observed with this nozzle (relative to the circular case; figure 7*a, b*) is consistent and comparable to that of the 16:1 case in figure 14. Thus, it is inferred that the effect of shear layer perimeter stretching on jet spreading with small aspect ratio asymmetric nozzles must be insignificant. To enable large spreading purely through perimeter stretching, one needs to stretch the mixing layer very significantly. With the dimensions of the present lobed nozzle, for example, many more lobes would be needed to achieve the same spreading as obtained by screech or tabs. Another way of expressing the perimeter stretching would be to form a ratio of the hydraulic diameter to the equivalent diameter ( $D_H/D$ ). Ratios for the 8:1, 16:1 and 32:1 orifices are 1.8, 2.4 and 3.29, respectively. From the data of figure 14, it may be concluded that at an aspect ratio of about 10 ( $D_H/D \approx 2$ ), the effect of perimeter stretching would yield a noticeable increase in the jet spreading; and again, for a significant increase in spreading much larger ratios would be needed.

What then caused the large entrainment in the low aspect ratio asymmetric jets reported in the literature (Ho & Gutmark 1987; Hussain & Husain 1989)? Recall the difference in the mass flux results between the present asymmetric jets (figure 7*a*) and that of Ho & Gutmark (1987), discussed earlier. A difference in the initial condition, i.e. initial boundary layer state, is thought to be a likely reason for this difference.

Recall the discussion (§ 3.2) that artificial excitation of an asymmetric jet leads to a pronounced spreading as well as a faster axis switching. It should be recognized that a similar mechanism is also operating in a natural asymmetric jet. There is always some natural excitation in any given jet. The natural excitation, however, varies depending on the initial and background conditions as well as the initial boundary layer state.

At low Mach and Reynolds numbers, in the jets of Ho & Gutmark (1987) and Hussain & Husain (1989), the initial boundary layer was laminar and the turbulence in the core of the jet was low. Such jets can be susceptible to small-amplitude background disturbances. It is as though these jets are prone to ‘self excitation’. With such a jet, there can be an organized roll-up of the azimuthal vorticity similar to what happens with an artificially excited jet. At  $M_j \geq 0.3$  with the present jets, on the other hand, the initial boundary layer is only nominally laminar and the fluctuation intensity within the boundary layer is high with a broadband energy spectrum (§ 2). In such a jet, the initial roll-up of the azimuthal vorticity may not be as organized, and randomness may prevail. Under those conditions, axis switching may not be observed clearly (or a delayed switching may occur), and the jet spreading may not be accentuated. This initial condition effect is vividly illustrated by the results of Hussain & Husain (1989). When they tripped the boundary layer of their elliptic jet, the axis switching location shifted from  $3.5D$  to  $15D$  and the spreading was significantly less (their figure 32). Therefore, a relatively ‘unclean’ initial condition with the present jets, practically inevitable at higher jet Mach numbers, is responsible for the lesser jet spreading.

Another factor that might have contributed to the difference in the jet spreading between the present and the cited works could be the difference in streamwise vorticity distribution at the nozzle exit. Streamwise vortices are expected owing to upstream secondary flow. Any nozzle contracting from one cross-sectional shape to another would be characterized by such vortices. The strength and sense of rotation of those vortices may depend on the detailed geometry of the nozzle (Zaman 1996*b*). A difference in the initial streamwise vorticity distribution can impact the downstream jet evolution quite significantly. In fact, this could explain the slightly larger fluxes with the asymmetric nozzles (figure 7*b*) as compared to the fluxes for the orifice cases (figure 14), since streamwise vorticity due to upstream secondary flow in the latter cases should be minimal. The role of the streamwise vortices on jet spreading is now further addressed.

### 3.4. Effect of streamwise vortex pairs on jet spreading

We have noted from figures 7 and 13 that the fluxes for the tab cases are much larger than those obtained with any of the asymmetric nozzles. This is true for supersonic as well as subsonic conditions. Furthermore, in the supersonic regime, the tabs eliminate screech and yet the spreading increase caused by them is by far the greatest. The effect of the tabs occurs through the dynamics of streamwise vortex pairs. This is elaborated in the following. First, evidence is presented showing that the tabs produce similar streamwise vortex pairs regardless of the jet Mach number.

#### 3.4.1. Streamwise vorticity in the tabbed rectangular jet

That a tab produces a pair of counter rotating streamwise vortices had been measured in several previous experiments with incompressible flows (Zaman *et al.* 1994; Bohl & Foss 1996; Reeder & Samimy 1996). That the corresponding vorticity distribution and dynamics are essentially similar in compressible flows had been conjectured from flow visualization of overall jet distortion (Zaman *et al.* 1994). This is further supported by numerical analysis of the tabbed rectangular jet case, carried out by the author’s two colleagues, C. J. Steffen and D. R. Reddy.

Figure 15(*a*) shows the streamwise vorticity distribution measured on the jet cross-sectional plane at  $x/D = 1$  and  $M_j = 0.3$ . These data were obtained by hot-wire anemometry for the 3:1 rectangular nozzle with tabs. The nozzle used for this experiment, however, was larger but geometrically similar to that shown in figure 1.

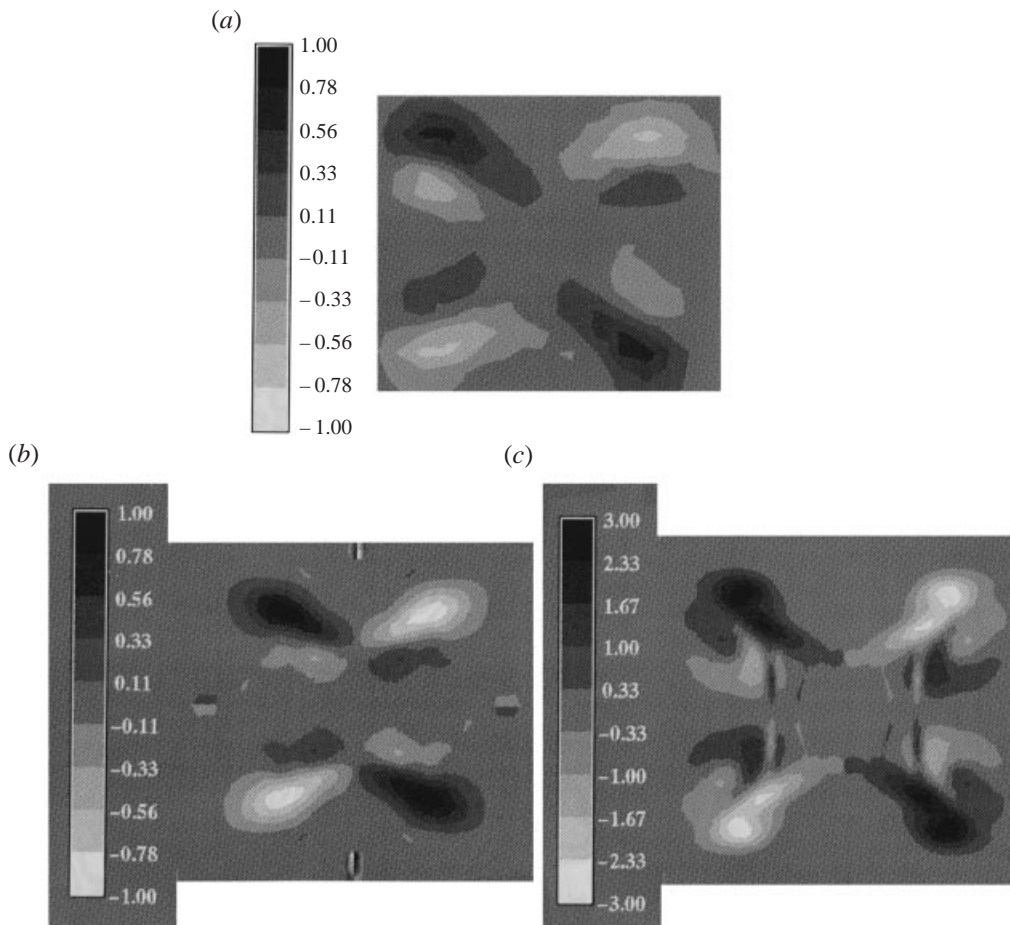


FIGURE 15. Normalized streamwise vorticity ( $\omega_x D/U_e$ ) distribution, on jet cross-sectional ( $y, z$ )-plane, at  $x/D = 1$  for the rectangular nozzle with tab case. (a) Measured data for  $M_j = 0.3$ , (b) computational result for  $M_j = 0.3$ , (c) computational result for  $M_j = 1.63$ .

The larger nozzle ( $D = 6.35$  cm,  $Re_D = 450\,000$ ) was needed from probe resolution considerations. Flow-field surveys showed essentially similar jet evolution, as discussed so far, at the higher  $Re_D$  both with and without tabs. With reference to past results, it can be inferred that the vortex pairs at the top and bottom of figure 15(a) are the primary pairs originating from the two tabs. (The nozzle major axis is vertical and the two tabs are located at the top and bottom.) There are two additional inner pairs of opposite sense, presumably originating from the reorientation of the approach boundary layer (Bohl & Foss 1996; Reeder & Samimy 1996).

The computational result for the streamwise vorticity distribution, corresponding to the conditions of figure 15(a), is shown in figure 15(b). The steady-state flow-field calculations were performed using a time-marching full Navier–Stokes code called NPARC. It was observed that the choice of turbulence model played a less significant role in capturing the overall characteristics of the vortices initially. This is presumably because the vortex pair from a tab originated mainly from pressure driven sources (§ 3.4.2). Other considerations, e.g. inflow/outflow boundary conditions catering to the ‘entrainment appetite’ of the jet and grid generation for the tabbed nozzle geometry,

were more difficult hurdles in the computation. For further details the reader is referred to Steffen *et al.* (1997) and Reddy *et al.* (1997).

It can be seen that the agreement of the overall distribution (figure 15*b*), as well as amplitudes, with the experimental (figure 15*a*) data is good. Even the secondary, inner vortices are captured reasonably by the computation. Corresponding computational results for the supersonic condition ( $M_j = 1.63$ ), for which there are no experimental data owing to the lack of a reliable measurement technique, is shown in figure 15(*c*). The distribution is similar to that observed at the subsonic condition. These results, for the first time, provide a proof that streamwise vortex pairs are indeed introduced by the tabs at supersonic conditions. There is a difference in the indicated amplitudes, but this is partly due to the velocity scale used in the non-dimensionalization (Reddy *et al.* 1997). Ignoring this difference, the streamwise vorticity distribution in the tabbed jet under consideration is inferred to be essentially similar at subsonic and supersonic conditions. The dynamics of these vortex pairs govern the jet evolution, which is, therefore, similar at subsonic and supersonic conditions.

#### 3.4.2. Dynamics of streamwise vortex pairs causing jet spreading

Each tab produces a pair of counter-rotating streamwise vortices. The sense of rotation of the pair is such that, between the two vortices, ambient fluid is ingested into the core of the jet ('in-flow' sense). The mechanism of how a tab produces such a vortex pair has been discussed by Zaman *et al.* (1994) and, more recently, in further detail by Bohl & Foss (1996). In summary, the primary source of vorticity is a 'pressure hill' formed upstream of the tab as a result of the fact that the approach flow is slowed down. The gradient of the lateral pressure distribution, together with the presence of the wall, generates the pair of streamwise vortices with the 'in-flow' sense. Vorticity shed from the edges of a delta-tab, whose source is again pressure gradients on the tab's surface, also contributes to the streamwise vorticity. Components  $\omega_y$  and  $\omega_z$  are reoriented to  $\omega_x$  by appropriate terms in the  $x$ -component of the vorticity transport equation. Component  $\omega_x$  from the latter source reinforces the vorticity from the 'pressure hill' when the tab is tilted downstream. Foss & Zaman (1999) clearly documented this additive effect and showed that, while the circulation generated on the cross-stream plane is the maximum when the tab is placed normal ( $90^\circ$ ) to the free stream,  $\omega_x$ -peak is maximum when the tab is tilted downstream with  $\phi \approx 135^\circ$  (figure 1*c*). Furthermore, when the tab is tilted upstream ( $\phi \approx 45^\circ$ ), not only are both circulation and  $\omega_x$ -peak smaller owing to the cancellation effect from the two sources, but the thrust loss is also greater. Flow blockage by the tabs, and thrust penalty, are discussed in §3.4.3.

The outer, primary vortex pairs seen in figure 15 are the in-flow pairs originating from the two tabs. These are two pairs of counter-rotating vortices with high intensity which dominate the flow downstream. The overall jet spreading caused by these vortices can be explained by the same reasoning that explains axis switching (Zaman 1996*b*). Owing to mutual induction, the two pairs first move towards the jet centreline. This is shown schematically on the left of figure 16. The inward motion, however, is restricted as the two pairs approach each other, and shortly downstream, they rearrange to form two 'out-flow' pairs. The latter pairs eject jet core fluid while vortex induced motion propels them laterally away from the jet axis. This is what causes the rapid axis switching as well as the large lateral spreading of the jet.

The spreading for the circular jet with tabs can also be explained in a similar manner. This is shown schematically on the right in figure 16. Four equally spaced tabs produce four in-flow pairs. At first, all move towards the jet axis. However,



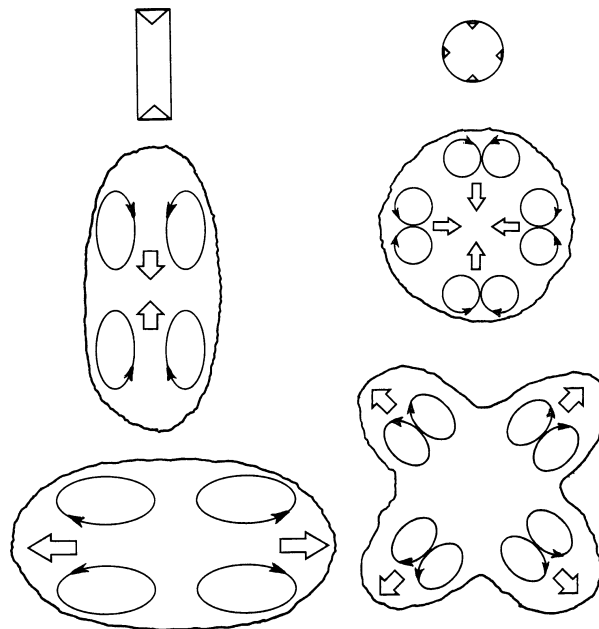


FIGURE 16. Schematic of streamwise vorticity distribution for the tab cases and their effect on jet spreading.

again, this motion is restricted and, shortly downstream, vortices from adjacent pairs form four 'out-flow' pairs. The subsequent motion of the 'out-flow' pairs causes the characteristic cross-sectional shapes (see the left cross-sectional cuts in figures 5 and 6), as well as the large spreading.

The vigour of the dynamics of the vortex pairs should depend on the strength and spacing of the vortices which in turn depends on the tab geometry. It is worth mentioning here that two smaller tabs placed on the narrow edges of the rectangular nozzle yielded significantly lower jet spreading (Zaman 1996*b*). For the two tab configurations, considered so far in this paper, the streamwise vortex dynamics are indeed quite vigorous. These resulted in the most pronounced jet spreading thus far observed in the investigation. Finally, it should be recognized that the induced motion of the steady vortex pairs explains the tendency for the jet cross-section to spread in a certain manner. Actual mixing and entrainment must involve unsteady motion at smaller scales. The latter issue is considered beyond the scope of the present paper; Liepmann & Gharib (1992), among others, have provided some insight in that regard.

### 3.4.3. Flow blockage and thrust loss due to the tabs

Since thrust loss is of prime concern in propulsion applications, the loss incurred by the tabs *vis-a-vis* the spreading increase is examined in this final section. Thrust was measured by a 'load-cell' with the plenum chamber mounted on linear bearings. Simultaneously, the mass flow rate through the nozzle was also measured by an orifice-meter installed on the air supply line. Further details of these measurements can be found in Zaman (1996*a*).

The ideal mass flow rate for the nozzle (without tabs),  $m_{ideal} = \rho_e A_e U_e$  was calculated from conditions at the nozzle exit assuming a 'top-hat' velocity profile and zero boundary-layer thickness; the density and velocity were obtained from the plenum-chamber-to-ambient pressure ratio. Comparison with the measured mass flow rate,







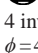

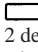
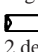
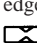
Case	Nozzle and tab configuration	Approximate tab width, $w/D$	Flow blockage (%)	Thrust loss (%)	Thrust co-efficient, $C_f$	Mass flux $\dot{m}/\dot{m}_e$ at $x/D_e = 14$	Maximum Mach number at $x/D_e = 14$	$\frac{\Delta \dot{m}}{1 - C_f}$
1	No tab 	0	0	0	1.00	3.12	0.86	—
2	4 delta, $\phi = 135^\circ$ 	0.14	1.1	4.1	0.971	3.28	0.79	1.8
3		0.21	2.6	7.6	0.948	4.59	0.58	9.0
4		0.28	6.2	15.6	0.913	5.58	0.50	9.1
5		0.43	14.1	23.7	0.889	5.70	0.47	7.5
6		0.57	26.5	38.4	0.838	5.89	0.42	5.5
7		0.62	46.3	54.7	0.844	5.91	0.37	5.7
8	4 inverted delta, $\phi = 45^\circ$ 	0.28	14.1	18.9	0.944	3.58	0.76	2.6
9	No tab 	0	2.4	2.7	0.998	3.88	0.55	—
10	2 delta on short edges 	0.53	8.1	12.9	0.948	5.63	0.39	15.5 (8.7)
11	2 delta on long edges 	0.53	13.5	20.1	0.924	4.12	0.50	4.2 (0.8)

TABLE 1. Flow blockage, jet spreading and thrust loss with different tab configurations, at  $M_j = 1.63$ .

$m_{meas}$ , provided the actual flow blockage for a given nozzle and tab configuration (% blockage =  $(m_{ideal} - m_{meas})/m_{ideal} \times 100$ ). For the purposes of the discussion in this section, an equivalent diameter,  $D_e = ((4/\pi)(m_{meas}/\rho_e U_e))^{1/2}$ , was calculated from the measured mass flow rate and the conditions at the nozzle exit. For each tab configuration, the nozzle exit area ( $A_e = \pi D_e^2$ ) was used to calculate an ideal thrust,  $T_{ideal}$ , using (2) of § 3.1. The thrust coefficient was then obtained as,  $C_f = T_{meas}/T_{ideal}$ . These measurements were performed for a given nozzle configuration followed by normalized mass flux measurement at  $x/D_e = 14$  (data as in figure 13). The sequence of measurement was repeated for a number of tab configurations as discussed below.

The first tab configurations examined were four equally spaced delta-tabs with the circular nozzle, the tab size having been varied systematically. With reference to figure 1(c),  $w/D$  was varied with approximate values: 0.14, 0.21, 0.28, 0.43, 0.57 and 0.62. These are listed as cases 2–7 in table 1, case 1 being without tabs. Note that only the  $w/D = 0.28$  size (case 4) has been considered so far for the circular nozzle. In addition, a case (8) with the latter four tabs placed inverted ( $\phi = 45^\circ$ ) is also examined. The rectangular nozzle with two delta-tabs on the short edges, the other tab case considered so far, and another case with the same two tabs located on the long edges of the nozzle, are also examined. These, and the corresponding no-tab configuration, are listed as cases 9–11 in table 1.

The measured thrust for cases 1–7 is shown in figure 17 as a function of the nozzle pressure ratio ( $p_t/p_a$ ). The variable  $p_t/p_a$  is chosen for the abscissa, instead of  $M_j$  because the thrust variation is then approximately linear and comparison becomes

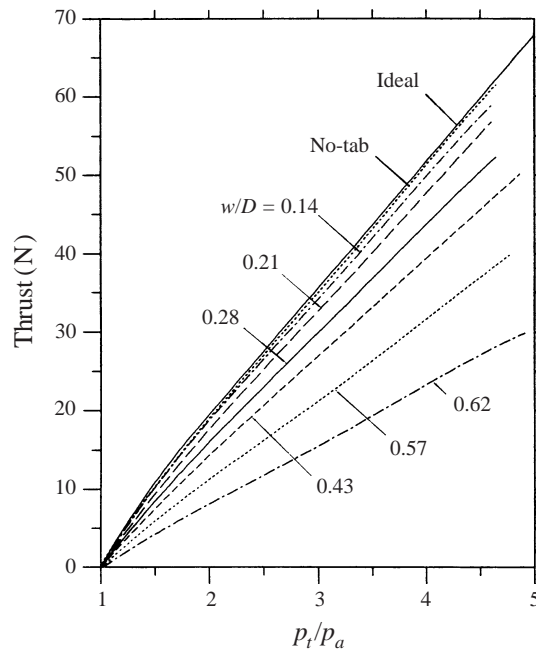


FIGURE 17. Thrust versus nozzle pressure ratio for the circular jet with and without four delta tabs. Different curves are for varying tab size  $w/D$  (figure 1(c) and table 1); the solid curve is the isentropic prediction for the no-tab case, assuming top-hat velocity profile.

easier. Also, for clarity, only least-squares fitted curves are shown; each curve is based on approximately 10 data points. Note that the curve marked 'ideal' represents ideal thrust assuming zero boundary-layer thickness for the no-tab case. The slightly lower thrust measured for the no tab case should be due to the boundary-layer effect. It is evident that with increasing size of the four delta-tabs there is increasing thrust loss. The measured loss relative to the no-tab ideal value in per cent for all the cases is listed in column 5 of table 1. These losses, calculated for  $p_t/p_a = 4.47$  ( $M_j = 1.63$ ), are representative of that at other nozzle pressure ratios. An inspection of cases 1–4 reveals that the thrust loss varies approximately linearly with the geometric area blockage imparted by the tabs; that is,  $\text{loss}/(w/D)^2 \approx \text{constant}$ . However, with further increase in the tab size the variation is no longer linear.

With increasing tab size, the flow rate also decreases for a given pressure ratio. The measured flow blockage is listed in column 4 of table 1. This and other quantities in table 1, calculated for  $p_t/p_a = 4.47$  ( $M_j = 1.63$ ), are also representative of corresponding values at other pressure ratios. An inspection of columns 3 and 4 makes it apparent that the measured flow blockage does not necessarily follow the geometric area blockage (which is proportional to  $(w/D)^2$ ), and depends, especially, on the orientation of the tab. For example, compare the data for cases 4 and 8. For the delta-tab ( $\phi = 135^\circ$ , case 4), the flow blockage (6.2%) can be found to be less than the geometric area blockage (about 8%). With same area blockage, the inverted tabs ( $\phi = 45^\circ$ , case 8) impart a much larger flow blockage. This is expected because in the latter case the flow upstream of the tab is halted, whereas in the former case the flow is merely deflected.

Since the thrust loss is accompanied by a decrease in the mass flow rate, an evaluation of the performance of a given nozzle and tab configuration is appropriate

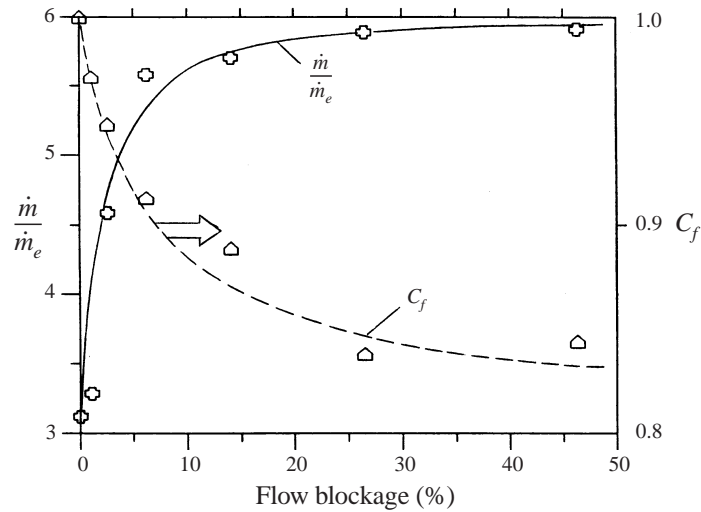


FIGURE 18. Effect of four delta tabs of varying size on the mass flux (at  $x/D_e=14$ ) and the thrust coefficient of the circular jet. Abscissa is measured flow blockage for the seven cases of figure 17.

only when the thrust coefficient is compared. The thrust coefficient is listed in column 6 of table 1. (As stated before,  $T_{ideal}$ , used to obtain  $C_f$ , was calculated by assuming convergent, uniform flow at the nozzle exit. For a given  $p_t/p_a$ , full expansion, via a convergent-divergent nozzle, would yield the maximum available thrust. This would be higher, for example, by about 2% at  $p_t/p_a = 4.47$ . If this were used in the calculation, the thrust coefficients would have correspondingly lower values. For the present study, comparison of  $C_f$  is deemed sufficient.) The variation of  $C_f$  for cases 1–7 is shown in figure 18 as a function of the flow blockage. A steep initial decrease in  $C_f$  with increasing tab size is apparent. However, with further increase in the size the curve levels off.

It should be noted that the height of even the smallest size tab is expected to be much larger than the nozzle boundary-layer thickness. (At subsonic conditions, the momentum thickness variation was found to follow the equation,  $\theta/D = 1.0/(Re_D)^{1/2}$ ; §2. Extrapolation of this relationship to  $p_t/p_a = 4.47$  ( $M_j = 1.63$ ,  $Re_D \approx 0.84 \times 10^6$ ) yields a momentum thickness of about  $0.001D$ . The protrusion of the smallest size tab was about  $0.05D$ .) As long as the tab height is large relative to the boundary-layer thickness, the same vorticity-generation mechanism as described in §3.4.2 should be operative. Thus, even the smallest size tab would produce a pair of streamwise vortices. The generation of streamwise vorticity, however, represents diversion of some of the axial momentum into the circulation on the cross-stream plane. Hence, there should be an accompanying drop in the thrust coefficient.

With increasing size of the delta-tab the magnitude of the circulation on the cross-stream plane for each element of the vortex pair may be expected to increase. This expectation is based on experimental evidence that the non-dimensional circulation is a constant. The circulation, non-dimensionalized by the approach velocity and the base width of the delta-tab, was measured to be about 0.1 by Foss & Zaman (1999). Corresponding values approximated from streamwise vorticity distributions published earlier, for an order-of-magnitude-larger tab by Bohl & Foss (1996), and for an order-of-magnitude-smaller tab by Zaman *et al.* (1994), were about the same. Thus, it would be expected that with increasing tab size, the circulation for a given

jet velocity would increase. This would be accompanied by a decrease in  $C_f$ . The data in figure 18 show that the rate of this decrease falls off with a further increase in tab size. This presumably occurs because of flow interaction from adjacent tabs. With a large size, an individual delta-tab no longer acts in a manner described in §3.4.2.

The normalized mass flux data, at  $x/D=14$ , were obtained following the thrust measurement without disturbing the tab configuration. These data, also shown in figure 18, exhibit a trend that is the reverse of that which occurs with  $C_f$ . There is a sharp increase in the flux value initially, but further increase in the tab size does not increase it as much. The curve levels off for tab size larger than about  $w/D=0.28$  (blockage of about 6%).

Thus, with increasing tab size, as stated in the foregoing, the streamwise vortices and the associated circulation on the cross-stream plane become stronger. Stronger cross-stream circulation yields increased jet spreading. However, this is achieved at the expense of increasing thrust loss. Furthermore, for a given nozzle, the tab size ( $w/D$ ) can be increased only up to a limit. Beyond that, there is flow interference from adjacent tabs, and, the rate of increase in the cross-stream circulation levels off. In turn, both rate of increase in jet spreading and rate of decrease in  $C_f$  also level off.

The increase in spreading versus the loss in thrust is described by a 'performance factor' listed in the last column of table 1. This quantity, defined as,

$$\frac{\Delta\dot{m}}{1 - C_f} = \left( \frac{\dot{m}_{tab} - \dot{m}_{no-tab}}{\dot{m}_{no-tab}} \right) / (1 - C_f),$$

represents the increase (%) in the mass flux at  $x/D = 14$  per decrease (%) in the thrust coefficient. It is merely used to summarize the overall effect and the reader is cautioned not to put too much emphasis on it, since with the tab size approaching zero it becomes indeterminate. Columns 6 and 7 already document how much gain in spreading has been achieved and at what cost. The 'performance factor' combines those effects. Based on this factor, it should be evident that the optimum size, for the four delta-tabs with the circular nozzle configuration, is around  $w/D = 0.28$ .

The data trend discussed so far in this section is based on the circular nozzle fitted with four delta-tabs of various size. The inference on the optimum size applies only for that and not other tab geometry. For example, when the same tabs ( $w/D = 0.28$ ) are placed inverted ( $\phi = 45^\circ$ , figure 1c), the performance becomes much poorer. This can be discerned from the data for case 8 in table 1. Table 1 also makes it clear that the configuration involving two delta-tabs on the short edges of the 3:1 rectangular nozzle, the other tab case considered in the previous sections, perform very well. Note that the 'performance factor' for this case would be 8.7 when using  $\dot{m}_{no-tab} = 3.88$ , the value for the rectangular nozzle without tabs. A more appropriate comparison is made when a common 'baseline' value of  $\dot{m}_{no-tab}$  is used for all cases. With  $\dot{m}_{no-tab} = 3.12$ , the value for the circular jet, the performance factor for case 10 is 15.5. It should be clear that when the same two delta-tabs are placed on the long edges (case 11), the tabs are too close, there is flow interference, and the performance is poor. The tab configuration in the last case also resists axis switching (Zaman 1996b) and the spreading is just barely more than that observed with the no-tab case.

#### 4. Concluding remarks

The comparative spreading characteristics of free jets from a set of nozzles of asymmetric geometry have been studied. The set includes a circular, a 3:1 rectangular, a 3:1 elliptic and a 6-lobed nozzle. In addition, two cases of tabbed nozzles, as well as a set

of rectangular orifices with varying aspect ratio, are also included in the comparison. Measurements have covered incompressible subsonic conditions to underexpanded supersonic conditions up to a jet Mach number of about 2.0. Tabs and the phenomenon of screech alter jet spreading within the developing region significantly.

At subsonic conditions, jet spreading with the elliptic, rectangular or lobed nozzle is found to be only slightly more than that with the circular nozzle. This observation contrasts with certain earlier works reporting a large increase in jet spreading with small aspect ratio elliptic nozzles. The reason for the difference is thought to be due to a difference in the initial conditions of the jets in the present and the previous studies. The jets in the previous studies, at low Mach and Reynolds numbers, involve initially laminar boundary layers with low free-stream turbulence. It is reasoned that such jets are susceptible to excitation by small-amplitude background disturbances. A state of natural 'self excitation' organizes the azimuthal vortical structures that lead to a more pronounced axis switching as well as higher entrainment. At higher Mach numbers covered in the present study the initial condition is relatively 'unclean'; thus, some amount of randomness prevails in the evolution of the azimuthal vortical structures. This leads to a delayed axis switching accompanied by lesser jet spreading. This notion is clearly supported by the elliptic jet data, with and without boundary-layer trip, provided by Hussain & Husain (1989). With the tripped boundary layer, compared to the no-trip case, the axis switching location moved farther downstream and the spreading of the jet was significantly less.

That the spreading of the asymmetric jets is not much different from that of a circular jet is further demonstrated by data from the rectangular orifices. An increased spreading is detected only when the aspect ratio is larger than about 10. Up to an aspect ratio of 8:1, the jet spreading characteristics are essentially indistinguishable from those of the circular jet. Thus, mixing-layer perimeter stretching, obtained by increasing the aspect ratio of a rectangular orifice for a given exit area, becomes effective only when the stretching is carried out to a large extent. In other words, 'shear layer perimeter stretching' by itself is an inefficient mechanism for increasing jet entrainment and spreading. A threshold for the perimeter stretching to become effective could be expressed in terms of the ratio of hydraulic to equivalent diameter. That ratio needs to be greater than about 2 to enable a noticeable increase in jet spreading.

In the supersonic regime, when screech occurs, jet spreading increases with all nozzles. Thus, the lobed nozzle, which does not involve screech, exhibits the least spreading in the supersonic regime. The amount of increase in spreading varies with the stage of the screech; the largest increase occurs with the stage involving flapping flow oscillation. The rectangular and elliptic nozzles involve only flapping mode screech; thus, spreading with these nozzles in the supersonic regime is generally higher than that of the circular case.

Jet spreading for the two tab configurations is found to be the largest among all the cases. This is true in the subsonic regime, as well as in the supersonic regime in spite of the fact that screech is eliminated by the tabs. The dynamics of streamwise vortex pairs produced by the tabs cause the most efficient jet spreading. Thus, a manipulation of the streamwise vortex pairs may hold the key for any further increase in jet spreading.

However, with the tabs there is a performance penalty. The spreading increase versus the performance loss is studied systematically for a number of tab configurations. With four equally spaced delta-tabs with the circular nozzle, optimal spreading with minimal thrust loss is achieved when each tab has a base width equal to about 28% of the nozzle diameter. The best tab case, observed so far, turns out to be the

3:1 rectangular nozzle with two large delta tabs on the short edges. Approximately 120 % increase in the entrained flow is observed at  $x/D = 14$  (normalized mass flux increasing from 3.12 to 5.63). The corresponding loss in the thrust coefficient is approximately 5 %.

The author would like to take this opportunity to acknowledge the many contributions of Mr John M. Abbott who has not only supported and encouraged this research as Branch Chief, but also provided valuable technical input as a colleague. Thanks are also due to Drs J. K. Foss Van Zante, G. Raman and J. Panda for helpful inputs as well as help with some of the data acquisition.

## REFERENCES

- AHUJA K. K. & BROWN W. H. 1989 Shear flow control by mechanical tabs. *AIAA Paper* 89-0994.
- BELOVICH, V. M., SAMIMY, M. & REEDER, M. F. 1996 Dual stream axisymmetric mixing in the presence of axial vorticity. *J. Propulsion Power* **12**, 178-185.
- BOHL, D. & FOSS, J. 1996 Enhancement of passive mixing tabs by the addition of secondary tabs. *AIAA Paper* 96-0545.
- BRADSHAW, P. 1987 Turbulent secondary flow. *Ann. Rev. Fluid Mech.* **19**, 53.
- COHEN, J. & WYGNANSKI, I. 1987 The evolution of instabilities in the axisymmetric jet. Part 2. The flow resulting from the interaction between two waves. *J. Fluid Mech.* **176**, 221-235.
- CROW, S. C. & CHAMPAGNE, F. H. 1971 Orderly structures in jet turbulence. *J. Fluid Mech.* **48**, 547.
- DAVIS, M. G. & OLDFIELD, D. E. S. 1962 Tones from a choked axisymmetric jet. I. Cell structure, eddy velocity and source locations. *Acustica* **12**, 257-277.
- FOSS, J. K. & ZAMAN, K. B. M. Q. 1999 Large and small scale vortical motions in a shear layer perturbed by tabs. *J. Fluid Mech.* **382**, 307.
- GLASS, D. R. 1968 Effects of acoustic feedback on the spread and decay of supersonic jets. *AIAA J.* **6**, 1890-1897.
- GRINSTEIN, F. F. 1995 Self-induced vortex ring dynamics in subsonic rectangular jets. *Phys. Fluids* **7**, 2519.
- GUTMAK, E. J. SCHADOW, K. C. & YU, K. H. 1995 Mixing enhancement in supersonic free shear flows. *Ann. Rev. Fluid Mech.* **27**, 375-417.
- HO, C.-M. & GUTMARK, E. 1987 Vortex induction and mass entrainment in a small-aspect-ratio elliptic jet. *J. Fluid Mech.* **179**, 383-405.
- HUSSAIN, A. K. M. F. & CLARK A. R. 1977 Upstream influence on the near field of a plane turbulent jet. *Phys. Fluids* **20**, 1416.
- HUSSAIN, F. & HUSAIN, H. S. 1989 Elliptic jets. Part 1. Characteristics of unexcited and excited jets. *J. Fluid Mech.* **208**, 257-320.
- KROTHAPALLI, A., BAGANOFF, D. & KARAMCHETI, K. 1981 On the mixing of rectangular jet. *J. Fluid Mech.* **107**, 201.
- KROTHAPALLI, A., HSIA, Y., BAGANOFF, D. & KARAMCHETI, K. 1986 The role of screech tones in mixing of an underexpanded rectangular jet. *J. Sound Vib.* **106**, 119-143.
- LASHERAS, J. C. & PRESTRIDGE, K. 1997 Three dimensional vorticity dynamics in coflowing jets subjected to axial and azimuthal forcing. *AIAA Paper* 97-1880.
- LIEPMANN, D. & GHARIB, M. 1992 The role of streamwise vorticity in the near-field entrainment of round jets. *J. Fluid Mech.* **245**, pp. 643-668.
- MCCORMICK, D. C. & BENNETT, J. C. 1993 Vortical and turbulent structure of a lobed mixer free-shear layer. *AIAA Paper* 93-0219.
- NORUM, T. D. 1983 Screech suppression in supersonic jet. *AIAA J.* **21**, 235-240.
- PANDA, J. 1995 Measurement of shock oscillation in underexpanded supersonic jets. *AIAA Paper* 95-2145.
- PAPAMOSCHOU, D. & ROSHKO, A. 1988 The compressible turbulent shear layer: an experimental study. *J. Fluid Mech.* **197**, 453-477.

- PAREKH, D. E., REYNOLDS, W. C. & MUNGAL, M. G. 1987 Bifurcation of round air jets by dual-mode acoustic excitation. *AIAA Paper* 87-0164.
- PONTON, M. K. & SEINER, J. M. 1995 Acoustic study of B helical mode for choked axisymmetric nozzle. *AIAA J.* **33**, 413–420.
- POWELL, A. 1953 On the mechanism of choked jet noise. *Proc. Phys. Soc. Lond.* B **66**, 1039.
- POWELL, A., UMEDA, Y. & ISHII, R. 1990 The screech of round choked jets, revisited. *AIAA Paper* 90–3980.
- RAMAN, G., RICE, E. J. & RESHOTKO, E. 1991 Control of an axisymmetric turbulent jet by multi-modal excitation. *Proc. 8th Turb. Shear Flow Conf.* 6-2, Technical University of Munich.
- REDDY, D. R., STEFFEN, C. J. & ZAMAN, K. B. M. Q. 1997 Computation of 3-D compressible flow from a rectangular nozzle with delta tabs. *ASME Gas Turbine Conf. Paper 97-GT-257*. Orlando.
- REEDER, M. F. & SAMIMY, M. 1996 The evolution of a jet with vortex-generating tabs: real-time visualization and quantitative measurements. *J. Fluid Mech.* **311**, 73–118.
- REEDER, M. F. & ZAMAN, K. B. M. Q. 1996 The impact of tab location relative to the nozzle exit on jet distortion. *AIAA J.* **34**, 197–199.
- RICOU, F. P. & SPALDING, D. B. 1961 Measurements of entrainment by axisymmetrical turbulent jets. *J. Fluid Mech.* **11**, 21–32.
- SAMIMY, M. & ELLIOTT, G. S. 1990 Effects of compressibility on the characteristics of free shear layers. *AIAA J.* **28**, 439–445.
- SCHADOW, K. C., WILSON, K. J., LEE, M. J. & GUTMARK, E. 1987 Enhancement of mixing in reacting fuel-rich plumes issues from elliptic nozzles. *J. Propulsion* **3**, 145.
- SEINER, J. M. 1984 Advances in high speed jet aeroacoustics. *AIAA Paper* 84-2275.
- SHERMAN, P. M., GLASS, D. R. & DULEEP, K. G. 1976 Jet flow field during screech. *Appl. Sci. Res.* **32**, 283–303.
- STEFFEN, C. J., REDDY, D. R. & ZAMAN, K. B. M. Q. 1997 Numerical modeling of jet entrainment for nozzles fitted with delta tabs. *AIAA Paper* 97-0709.
- STRANGE, P. J. R. & CRIGHTON, D. G. 1983 Spinning modes on axisymmetric jets. Part 1. *J. Fluid Mech.* **134**, 231–245. (Also, PhD. thesis of P.J.R.S. University of Leeds, UK, 1981).
- SURKS, P., ROGERS, C. B. & PAREKH, D. E. 1994 Entrainment and acoustic variations in a round jet from introduced streamwise vorticity. *AIAA J.* **32**, 2108–2110.
- TAM, C. K. W. 1991 Jet noise generated by large-scale coherent motion. *NASA RP* 1258, vol 1.
- TRENTACOSTE, N. & SFORZA, P. 1967 Further experimental results for three-dimensional free jets. *AIAA J.* **5**, 885–891.
- TSUCHIYA, Y., HORIKOSHI, C. & SATO, T. 1986 On the spread of reactangular jets. *Exps. Fluids* **4**, 197.
- WITZE, P. O. 1974 Centerline velocity decay of compressible free jets. *AIAA J.* **12**, 417.
- ZAMAN, K. B. M. Q. 1986 Flow field and near and far sound field of a subsonic jet. *J. Sound Vib.* **106**, 1–16.
- ZAMAN, K. B. M. Q. 1996a Spreading characteristics and thrust of jets from asymmetric nozzles. *AIAA Paper* 96-0200.
- ZAMAN, K. B. M. Q. 1996b Axis switching and spreading of an asymmetric jet; the role of coherent structure dynamics. *J. Fluid Mech.* **316**, 1–27.
- ZAMAN, K. B. M. Q. & RAMAN, G. 1997 Reversal in spreading of a tabbed circular jet under controlled excitation. *Phys. Fluids* **9**, 3733–3741.
- ZAMAN, K. B. M. Q., REEDER, M. F. & SAMIMY, M. 1994 Control of an axisymmetric jet using vortex generators. *Phys. Fluids A* **6**, 778–793.
- ZAMAN, K. B. M. Q., STEFFEN, C. J. & REDDY, D. R. 1997 Entrainment and spreading characteristics of jets from asymmetric nozzles. *AIAA Paper* 97–1878.
- ZHANG, S. & SCHNEIDER, S. P. 1995 Quantitative molecular-mixing measurements in a round jet with tabs. *Phys. Fluids* **7**, 1063–1070.